KAB

NORSAR

ROYAL NORWEGIAN COUNCIL FOR SCIENTIFIC AND INDUSTRIAL RESEARCH

Scientific Report No. 1-75/76

SEMIANNUAL TECHNICAL REPORT
NORSAR PHASE 3

1 July – 31 December 1975

Prepared by
K. A. Berteussen

Kjeller, 13 February 1976

Sponsored by
Advanced Research Projects Agency
ARPA Order No. 2551

REPORT DOCUMENTATION PAGE		READ INSTRUCTIONS BEFORE COMPLETING FORM
1. REPORT NUMBER F08606-76-C-0001	2. GOVT ACCESSION NO.	3. RECIPIENT'S CATALOG NUMBER
4. TITLE (and Subtitle) Semiannual Technical Report		5. TYPE OF REPORT & PERIOD COVERED Semiannual Technical 1 July - 31 December 75 6. PERFORMING ORG. REPORT NUMBER Scientific Rep. No. 1-75/76
7. AUTHOR(s) K.A. Berteussen (Editor)		8. CONTRACT OR GRANT NUMBER(s) F08606-76-C-0001
9. PERFORMING ORGANIZATION NAME AND ADDRESS NTNF/NORSAR Post Box 51, N-2007 Kjeller, Norway		10. PROGRAM ELEMENT, PROJECT, TASK AREA & WORK UNIT NUMBERS NORSAR Phase 3
11. CONTROLLING OFFICE NAME AND ADDRESS VELA Seismological Center 312 Montgomery Street Alexandria, Va. 22314		12. REPORT DATE 29 January 1976 13. NUMBER OF PAGES 75
14. MONITORING AGENCY NAME & ADDRESS(if different from Controlling Office)		15. SECURITY CLASS. (of this report) 15a. DECLASSIFICATION/DOWNGRADING SCHEDULE

16. DISTRIBUTION STATEMENT (of this Report)

APPROVED FOR PUBLIC RELEASE, DISTRIBUTION UNLIMITED.

17. DISTRIBUTION STATEMENT (of the abstract entered in Block 20, if different from Report)

18. SUPPLEMENTARY NOTES

19. KEY WORDS (Continue on reverse side if necessary and identify by block number)

20. ABSTRACT (Continue on reverse side if necessary and identify by block number)

This report covers research and operation activities at the Norwegian Seismic Array (NORSAR) for the period 1 July - 31 December 1975.

The different systems at the array have performed satisfactorily in the period (Chapter II), except for the Special Processing System (SPS) which has shown a more and more deteriorating performance. This situation is probably not going to improve

with time, and measures should therefore be taken to establish a backup system and/or to replace this problematic unit. Extensive tests have been run with a new version of the Detection Processor (DP), exchanging messages with the Communications and Control Processor located at the Seismic Data Analysis Center (SDAC), Alexandria, over the ARPANET. The total number of events reported this period is somewhat smaller than previous periods (Chapter III), which can be explained by the lack of larger seismic swarms. In the DP an automatic 'possible explosion' and 'large event' warning has been implemented (Chapter IV).

The period is characterized by a stable and satisfactory operation of the array instrumentation (Chapter V), resulting in a normal maintenance activity. In this period 14 papers, 1 report and 8 new programs have been finished (Chapter VI).

Chapter VII summarizes the research activities in the period, and altogether 10 different topics are covered. First a study of the upper mantle beneath Fennoscandia and Western Russia is presented. Then comes an investigation of the 3-dimensional structure under LASA and central California. The corresponding investigation for NORSAR was described in the report for the period 1 July 1974 - 30 June 1975. A new contribution to the discussion about the precursors to P'P' is found in Section VII.3, while Section VII.4 describes an analysis of Rayleigh waves from Novaya Zemlya explosions. Two studies of operational capabilities have been made, one for NORSAR, using three years of data, and one for a set of Fennoscandian stations, using six years of data. The purpose of the investigation presented in Section VII.7 is to estimate the M_s-m_b relationship for earthquakes and assess the impact of network magnitude bias effects on the results. A new earthquake-explosion discriminant, replacing M_s with the long period power spectrum estimate, is given in Section VII.8. Section VII.9 describes the last results on a study of seismicity in Fennoscandia, while Section VII.10 describes a project for precise monitoring of seismic velocities.

AFTAC Project Authorization No.:		VT/6702/B/ETR
ARPA Order No.	:	2551, Ammendment 8
Program Code No.	:	6F10
Name of Contractor	:	Royal Norwegian Council for Scientific and Industrial Research
Effective Date of Contract	:	1 July 1975
Contract Expiration Date	:	30 June 1976
Contract No.	:	F08606-76-C-0001
Project Manager	:	Nils Marås (02) 71 69 15
Title of Work	:	Norwegian Seismic Array (NORSAR) Phase 3
Amount of Contract	:	$800 000
Contract period covered by the report	:	1 July 1975 - 31 December 1975

This research was supported by the Advanced Research Projects Agency of the Department of Defense and was monitored by AFTAC/VSC, Alexandria VA 22313, under Contract No. F08606-76-C-0001.

TABLE OF CONTENTS

I SUMMARY

This report covers research and operation activities at the Norwegian Seismic Array (NORSAR) for the period 1 July - 31 December 1975.

The different systems at the array have performed satisfactorily in the period (Chapter II), except for the Special Processing System (SPS) which has shown a more and more deteriorating performance. This situation is probably not going to improve with time, and measures should therefore be taken to establish a backup system and/or to replace this problematic unit. Extensive tests have been run with a new version of the Detection Processor (DP), exchanging messages with the Communications and Control Processor located at the Seismic Data Analysis Center (SDAC), Alexandria, over the ARPANET. The total number of events reported this period is somewhat smaller than previous periods (Chapter III), which can be explained by the lack of larger seismic swarms. In the DP an automatic 'possible explosion' and 'large event' warning has been implemented (Chapter IV).

The period is characterized by a stable and satisfactory operation of the array instrumentation (Chapter V), resulting in a normal maintenance activity. In this period 14 papers, 1 report and 8 new programs have been finished (Chapter VI).

Chapter VII summarizes the research activities in the period, and altogether 10 different topics are covered. First a study of the upper mantle beneath Fennoscandia and Western Russia is presented. Then comes an investigation of the 3-dimensional structure under LASA and central California. The corresponding investigation for NORSAR was described in the report for the period 1 July 1974 - 30 June 1975. A new contribution to the discussion about the precursors to P'P' is found in Section VII.3, while Section VII.4 describes an analysis of Rayleigh waves from Novaya Zemlya explosions. Two studies

of operational capabilities have been made, one for NORSAR, using three years of data, and one for a set of Fennoscandian stations, using six years of data. The purpose of the investigation presented in Section VII.7 is to estimate the M_s-m_b relationship for earthquakes and assess the impact of network magnitude bias effects on the results. A new earthquake-explosion discriminant, replacing M_s with the long period power spectrum estimate, is given in Section VII.8. Section VII.9 describes the last results on a study of seismicity in Fennoscandia, while Section VII.10 describes a project for precise monitoring of seismic velocities.

II. OPERATION OF ALL SYSTEMS

II.1 Detection Processor Operation (DP)

The overall goal of having minimum system down time for the Detection Processor System has in this period to a small extent been in conflict with the demands for testing out the new version of the system as the 'primary online' system. This was especially felt towards the end of the period. Apart from this, hardware problems have mainly been the causes of breaks in the recording. The up time percentage is 97.3%, as compared to 99.2% for the previous reporting period (July 1974 to June 1975).

Fig. II.1.1 and the accompanying Table II.1.1 both show the daily DP down time in hours for the days between 1 July and 31 December 1975. The monthly recording times and up percentages are given in Table II.1.2.

The most significant break in the recording occurred on 3 to 4 September, when a hardware error in the SPS Multiplexer caused a down period of more than 41 hours. Also, thermal problems caused the SPS to stop 26 and 27 December for more than 16 hours, while a faulty core component caused an SPS stop of 21 hours 29 and 30 December. From Table II.1.2 we see that we in July had 41 stops and a mean time between failures of only 0.7 days. The main cause of these frequent stops was that the DP did not receive an interrupt from the SPS (Special Processing System) within the required time span.

The 115 breaks can be grouped in the following cateogries:

SPS Problems	:	45
Test	:	18
Hardware malfunction (air condition, CPU, 1052)	:	11
Power breaks & jumps	:	10
Unknown reason	:	7
Disk drive problems	:	6

Maintenance (lines or CE)	:	5
Tape drive problems	:	4
Software problems	:	3
TOD unit problems	:	2
ARPANET TIP	:	2
Program change	:	1
Operator error	:	1

The 'Tests' category consists of relatively small breaks in the recording, when the new, experimental DP was taken up as the 'primary' system. Conclusively, it is evident from this that malfunctioning or breakdown of the SPS is the cause of most of the breaks in recording, and also causes the longest breaks. It is not reasonable to believe that this situation will improve with time. Measures should therefore be taken to counteract an overall deteriorating performance of the system. One way of doing this would be to create a backup system capable of data recording, to be taken up when the SPS for some reason went down.

The total down time for this period was 129 hours 25 minutes. The mean time between failures for the period was 1.6 days, as compared with 2.8 days for the last reporting period (July 1974 to June 1975).

II.2 Event Processor Operation (EP)

Apart from one hangup, caused by DP writing garbage into the Shared Disk Time/Tape file during a re-initialization, the Event Processor has performed satisfactorily during this period. Its up time percentage is 25.5%, as compared with 29.8% for the last reporting period (July 1974 to June 1975) (see Table II.1.2). The computer time per processed event is, however, almost exactly the same.

Table II.1.1
(Sheet 1 of 3)

Days with break between 1600 - 0800

LIST OF BREAKS IN DP PROCESSING THE LAST HALF-YEAR

DAY	START		STOP		COMMENTS.....	
182	21	59	24	0	COMMUNICATIONS MAINT	I
182	0	0	0	2	COMMUNICATIONS MAINT	
185	15	42	15	52	SPS INTER NOT RECEIVED	
185	16	27	16	34	SPS INTER NOT RECEIVED	I
185	16	47	17	1	SPS INTER NOT RECEIVED	
189	14	20	15	15	1052 TYPEWRITER A TO B	
190	4	36	4	52	CUSTOMER ENGINEERING	I
190	20	17	20	58	UNKNOWN REASON	I
191	21	39	22	24	DISK DRIVE ERROR	I
192	3	50	4	27	DISK DRIVE ERROR	
192	23	6	23	26	DISK DRIVE ERROR	I
193	0	26	0	48	DISK DRIVE ERROR	
193	0	54	1	29	DISK DRIVE ERROR	
193	8	25	8	41	1052 ERROR A TO B	
193	15	59	19	21	SPS SYS LIGHT ON	
195	8	44	9	3	SPS INTER NOT RECEIVED	
195	11	52	11	58	SPS INTER NOT RECEIVED	
195	13	32	13	44	SPS INT NOT REC, B TO A	
195	14	0	14	11	SPS INTER NOT RECEIVED	
196	4	29	4	39	SPS INTER NOT RECEIVED	I
196	5	32	5	50	SPS INTER NOT RECEIVED	
196	6	10	6	18	SPS INTER NOT RECEIVED	
196	6	53	7	0	SPS INTER NOT RECEIVED	
196	14	20	14	42	POWER JUMP	
197	1	43	1	56	SPS INTER NOT RECEIVED	I
197	2	11	2	16	SPS DATA OVERFLOW	
197	14	40	14	43	TOD FAILURE	
198	1	51	1	55	SPS INTER NOT RECEIVED	I
198	2	46	2	52	SPS INTER NOT RECEIVED	
198	3	5	3	16	SPS INTER NOT RECEIVED	
198	3	20	3	51	SPS INTER NOT RECEIVED	
201	8	50	8	55	SPS INTER NOT RECEIVED	
201	9	39	9	45	SPS INTER NOT RECEIVED	
201	10	46	10	51	SPS INTER NOT RECEIVED	
207	23	39	23	56	SPS INTER NOT RECEIVED	I
208	0	5	0	27	SPS INTER NOT RECEIVED	
208	13	14	13	26	SPS INTER NOT RECEIVED	
208	13	52	14	21	SPS INTER NOT RECEIVED	

Table II.1.1
(Sheet 2 of 3)

LIST OF BREAKS IN DP PROCESSING THE LAST HALF-YEAR

DAY	START		STOP		COMMENTS.....
208	15	42	16	26	SPS INTER NOT RECEIVED
209	1	2	1	38	SPS INTER NOT RECEIVED
212	17	50	19	59	POWER FAIL, A TO B
212	22	13	22	44	MACHINE CHECK,CPU-B BAD
213	4	11	6	44	MACHINE CHECK,CPU-B BAD
213	8	26	8	30	B TO A
218	6	34	7	27	MACHINE ERROR,RED LGHTS
222	14	40	16	6	AIR CONDITION DOWN
223	9	50	10	5	BAD AIR CONDITION
223	10	20	11	4	BAD AIR CONDITION
223	11	9	11	40	BAD AIR CONDITION
223	12	16	12	29	BAD AIR CONDITION
225	15	40	15	57	SPS INTER NOT RECEIVED
226	13	17	13	35	PROGRAM UPDATE
234	23	59	24	0	UNKNOWN REASON
235	0	0	0	24	UNKNOWN REASON
236	7	21	7	40	UNKNOWN REASON
239	19	46	20	17	POWER JUMP
239	22	4	22	14	POWER ON B CAUSED STOP
240	8	25	8	57	POWER ON B CAUSED STOP
246	2	4	24	0	SPS MULTIPLEXER
247	0	0	19	5	SPS MULTIPLEXER
248	11	49	12	1	TEMP FRAME 1 SPS
249	22	9	22	29	MT 250 EOT NOT SENSED
265	9	1	9	41	MAINT ON 1052
267	10	14	10	31	MT 163 EOT NOT SENSED
269	16	7	16	28	PLOT TASK TROUBLE
270	0	19	0	29	TEMP FRAME 1,SPS
270	0	34	1	33	TEMP FRAME 1,SPS
270	10	36	11	7	TIP MAINTENANCE
271	1	39	1	54	TEMP FRAME 1 , SPS
271	2	14	2	57	TEMP FRAME 1 , SPS
271	3	16	4	14	TEMP FRAME 1 , SPS
271	4	30	4	50	TEMP FRAME 1 , SPS
271	5	4	8	5	TEMP FRAME 1 , SPS
273	9	13	9	39	DISK PACK MAINTENANCE
276	7	52	8	5	MAINT ON MT 160
276	18	17	19	6	OPERATOR ERROR

Table II.1.1
(Sheet 3 of 3)

LIST OF BREAKS IN DP PROCESSING THE LAST HALF-YEAR

DAY	START		STOP		COMMENTS.....
279	15	15	15	29	UNKNOWN
288	7	7	7	20	UNKNOWN REASON
290	12	57	13	14	UPDATE FROM B INTERFERE
292	2	2	2	19	UNKNOWN REAAON
295	4	9	4	27	UNKNOWN REAAUN
304	20	10	20	21	CHANGE OF TAPE DRIVES
307	15	35	15	40	CHANGE OF TAPE DRIVES
312	2	13	2	26	PLOT TASK TROUBLE
321	2	35	4	17	POWER JUMP
326	23	15	24	0	POWER JUMP
327	0	0	0	16	POWER JUMP
327	0	25	0	43	POWER JUMP
329	1	10	2	18	TIP TROUBLE
337	4	40	5	44	POWER JUMP
337	5	53	6	5	POWER JUMP
337	9	25	9	40	DISK ERROR
339	15	46	15	57	SDAC TEST
339	20	58	21	33	SDAC TEST
342	16	2	16	38	SDAC TEST
342	20	12	20	21	SDAC TEST
344	16	22	16	37	SDAC TEST
344	18	35	18	45	SDAC TEST
344	20	35	20	40	SDAC TEST
346	15	56	16	2	SDAC TEST
346	17	5	17	21	SDAC TEST
346	17	51	17	57	SDAC TEST
346	19	53	20	0	SDAC TEST
351	15	53	16	0	SDAC TEST
351	19	18	19	53	SDAC TEST
351	23	15	23	31	SDAC TEST
351	23	59	24	0	SDAC TEST
352	0	0	0	13	SDAC TEST
352	0	29	0	49	SDAC TEST
352	15	55	16	0	SDAC TEST
352	19	1	19	25	SDAC TEST
360	10	9	13	10	SPS THERMAL PROBLEMS
360	13	23	14	51	SPS THERMAL PROBLEMS
360	16	34	20	23	SPS THERMAL PROBLEMS
360	22	39	23	32	SPS THERMAL PROBLEMS
360	23	40	24	0	SPS THERMAL PROBLEMS
361	0	0	1	26	SPS THERMAL PROBLEMS
361	6	49	10	3	SPS THERMAL PROBLEMS
361	10	11	12	7	SPS THERMAL PROBLEMS
363	16	14	24	0	SPS HARDWARE ERROR
364	0	0	13	17	SPS HARDWARE ERROR
365	23	40	24	0	NEW YEAR STOP

Total 33 days with stop due to

Table II.1.2

DP & EP Computer Usage July-December 1975

MONTH	DP UPTIME (HRS)	DP UPTIME (%)	NO. OF DP BREAKS	NO. OF DAYS WITH DP BREAKS	DP MTBF (DAYS)	EP UPTIME (HRS)	EP UPTIME (%)
JUL	732.8	98.5	41	16	0.7	209	28.1
AUG	734.4	98.7	15	11	2.0	221	29.7
SEP	669.8	93.0	15	10	1.9	175	24.3
OCT	741.5	99.7	8	7	3.9	171	23.0
NOV	715.5	99.4	6	6	5.0	180	25.0
DEC	700.5	94.2	30	12	1.0	172	23.1
	4294.5	97.3	115	62	1.6	1128	25.5

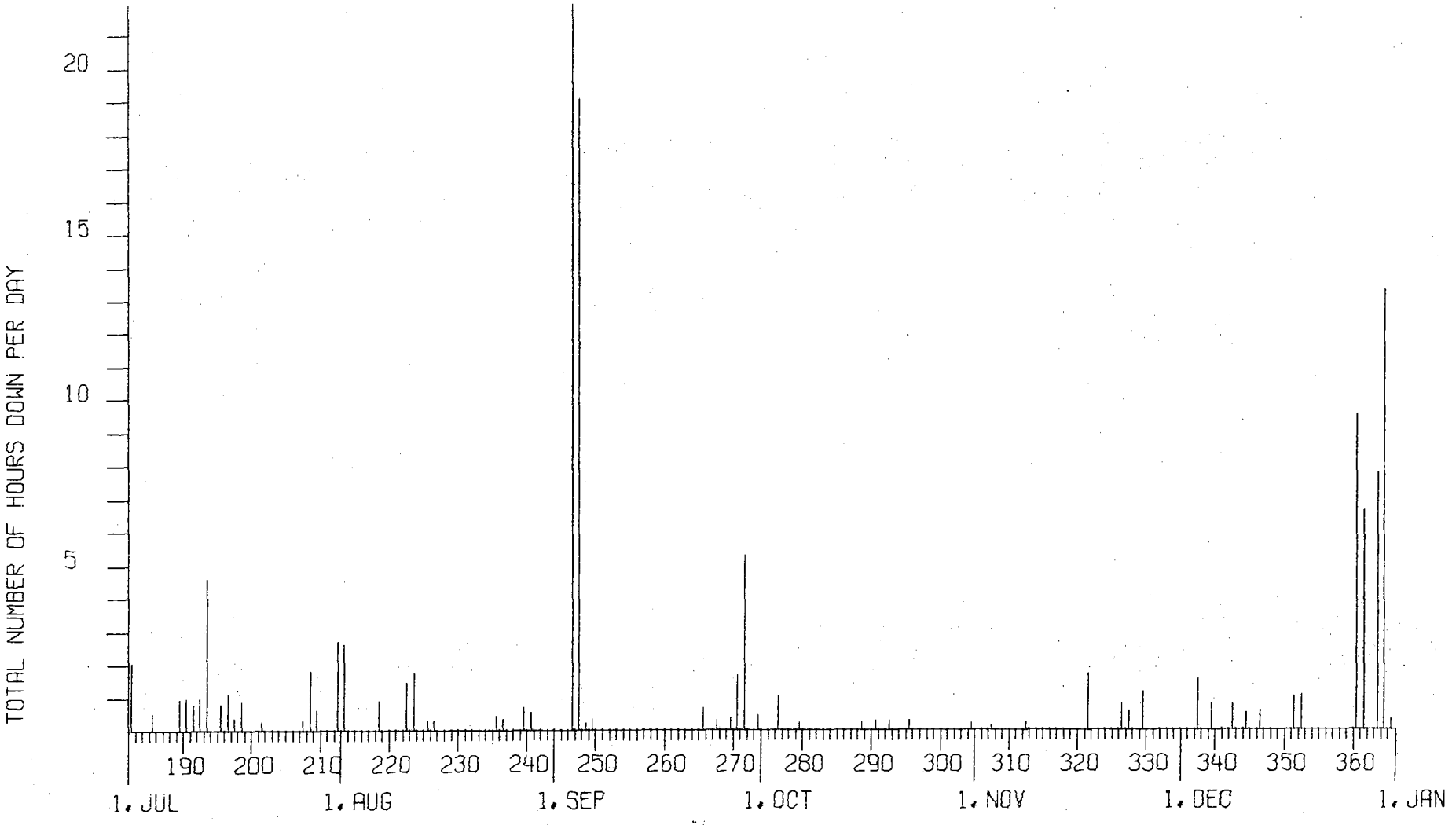

Fig. II.1.1 Detection Processor down time in the period
1 July - 31 December 1975

II.3 NORSAR Data Processing Center (NDPC) Operation

Data Center

No change in operational procedures, equipment configuration or facilities occurred in the report period.

Maintenance of equipment also continued as before, mainly performed by subcontractors for the different categories of equipment. Project personnel perform maintenance on some of the special equipment not covered by standard contracts.

Equipment performance in general was reasonably stable, as indicated by a Detection Processor up-time of 97.3% for the period. Of the remaining 2.7%, 0.2% is accounted for by power failure, 2% by Special Processing System (SPS) failure. Peripheral equipment have a somewhat higher failure rate, although usually with no serious effect on essential functions.

The SPS continues to cause some concern. It has had a series of - so far - unexplained stops. On one occasion (Dec 30) a faulty component was found (stops have also occurred since). It should be pointed out that, because of the complexity and uniqueness of this machine, local expertise is rather limited.

The ARPANET Terminal Interface Processor (TIP) and the 360/TIP interface units have performed satisfactorily. Minor modifications to the TIP were performed by Bolt Beranek and Newman Inc. (BBN) personnel in August and again in September.

Communications

The subarray communications system had about 'normal' outage compared to the long-term average. A few stations (04C, 07C and 13C) had longer outages caused by broken ground cables. The high outage figure for 01C is caused by power failure

(broken ground cable) rather than communications line fault (Table II.3.1).

An extensive program for remeasuring and reconditioning of communications circuits to conform with CCITT M102 specifications, in cooperation with the Norwegian Telegraph Administration (NTA), is in progress.

The international circuits (London, SDAC) appear to be stable, with only short and occasional breaks being observed. No statistics for these circuits are being kept, as no automatic registration is being performed here.

Table II.3.1

Communications, degraded performance (>20)/outages (>200).
Figures in per cent of total time. Month = 4 or 5 week periods as indicated.

Sub-array	JUL(5) >20	JUL(5) >200	AUG(4) >20	AUG(4) >200	SEP(4) >20	SEP(4) >200	OCT(5) >20	OCT(5) >200	NOV(4) >20	NOV(4) >200	DEC(4) >20	DEC(4) >200	AVG. ½YR >20	AVG. ½YR >200
01A	0.1	0.1	0.3	0.1	0.1	0.3	0.1	0.2	-	-	-	-	0.1	0.1
01B	0.2	3.6	0.2	0.3	0.2	0.3	0.1	0.2	-	0.1	-	-	0.1	0.8
02B	-	0.1	0.3	0.1	0.2	0.2	0.1	0.3	-	-	-	5.8	0.1	1.1
03B	0.2	0.1	0.4	0.2	1.0	0.3	2.8	0.4	0.6	0.1	-	-	0.8	0.2
04B	-	0.1	0.9	0.5	0.2	0.2	-	0.2	-	-	-	-	0.2	0.2
05B	0.3	0.1	0.3	0.2	0.2	0.2	0.4	14.4	0.3	2.7	-	2.7	0.3	3.1
06B	0.6	0.1	0.7	0.5	0.3	6.8	0.3	2.5	0.2	2.4	0.3	0.2	0.4	2.1
07B	0.6	0.3	0.4	3.0	0.6	0.2	0.2	0.2	0.2	8.0	0.2	0.2	0.4	2.0
01C	-	100	-	88.2	0.2	0.7	0.2	3.1	0.2	1.2	0.1	-	0.1	32.2
02C	0.1	0.1	0.4	0.6	0.3	0.4	0.2	1.3	0.1	0.4	0.2	0.1	0.2	0.5
03C	0.1	0.1	0.3	0.9	0.2	0.2	0.4	0.7	-	-	-	-	0.2	0.3
04C	0.3	0.1	0.2	23.8	0.2	0.8	0.1	0.3	-	0.3	0.1	-	0.2	4.2
05C	0.2	0.1	0.2	-	0.4	0.5	0.1	1.2	-	0.1	0.1	-	0.2	0.3
06C	0.1	0.1	0.2	0.1	0.2	0.2	0.1	0.1	-	-	-	-	0.1	0.1
07C	0.8	61.4	5.5	-	4.8	0.1	2.8	1.3	-	24.2	-	-	2.3	14.5
08C	0.1	1.6	0.1	-	-	-	-	0.1	0.1	-	-	-	0.1	0.3
09C	0.3	0.3	0.2	0.5	0.7	0.6	0.2	0.3	0.4	1.3	0.2	0.3	0.3	0.6
10C	0.7	3.3	0.2	0.5	0.8	0.9	0.5	3.9	0.6	3.2	0.3	0.5	0.5	2.1
11C	0.4	0.1	4.9	1.9	25.4	1.2	10.5	1.2	5.3	4.0	0.6	0.2	7.9	1.4
12C	0.7	0.1	0.6	0.2	0.3	0.4	0.3	0.3	0.2	14.0	0.2	0.2	0.4	2.5
13C	0.7	0.1	0.5	0.3	3.6	2.9	0.2	5.0	-	17.7	0.1	15.4	0.9	6.9
14C	-	0.1	0.2	0.2	0.2	0.3	0.2	0.3	0.2	0.9	0.3	0.2	0.2	0.3
AVG.	0.3	7.8	0.8	5.6	1.8	0.8	0.9	1.7	0.4	3.7	0.1	1.1	0.7	3.5
Less 01C		3.4		1.6										2.1

II.4 ARPANET

During the reporting period NORSAR has had the following attachments to the Terminal Interface Processor (TIP) located in the NORSAR Data Processing Center:

- Two terminals,
  Tektronix 4010-1 and
  Data Dynamics 390
- Two Special Host Interfaces,
  attached to Standard Host Interfaces 0 and 3 in the TIP.

The terminals have routinely been used for bulletin and data transfer, as well as for message exchange, the latter especially in connection with testing and debugging of the new seismic data exchange (see below). The terminal activity has been based upon our account at the OFFICE-1 host computer, as well as an account on the SRI-AI host computer. Both these ARPANET Hosts are located at Stanford, California.

Throughout the period extensive tests have been run with a new version of the Detection Processor (DP) System exchanging messages with the Communications and Control Processor located at SDAC, Alexandria, over the ARPANET. The new DP version incorporates a Network Control Program (NCP) as an extra task, enabling it to use ARPANET as a communication medium, instead of the old Trans-Atlantic (TAL) line, which was based on communication exchange between two SPS systems. As one expected, the tests helped to track down various errors in the format and content of the exchanged messages. One major problem encountered was the transmission delay related to the limited bandwidth available, especially during peak hours with heavy traffic. This delay caused intolerable buildup of waiting messages in both ends and consequent gaps in the transmission.

This problem was, however, solved by an IMP software modification which increased the available bandwidth sufficiently for the time being. Towards the end of the period, the new DP system was run repeatedly as "Primary Online", being able to communicate short period data requests from SDAC to the SPS, as well as forwarding Event Processor results to SDAC. Apart from some bug preventing the latter function to be performed correctly, the exchange works reasonably well for long periods of time. However, the major remaining problem is scarcity of queue storage in the DP system, and how this is distributed among the various queue block sizes at system start-up. Presently the situation is unstable, causing the system to terminate when demands for queue blocks are critical but cannot be fulfilled. The situation might be improved by trying to make more queue storage available, as well as preventing the system from terminating when the consequences of this does not influence the overall performance seriously (e.g., some non-critical message not printed).

III. ARRAY PERFORMANCE

Some basic statistics on the EP operation are given in Table III.1, which shows the analyst decisions for all the DP detections processed by EP during the reporting period. The percentages are quite close to those from the previous reporting periods, although the total number is somewhat smaller, which can be explained by the lack of larger seismicity swarms. This is seen from Fig. III.1, where the number of events on a daily basis is shown. On a monthly basis, the results are given in Table III.2.

With respect to detection and location capabilities, we refer to Section VII.5.

Table III.1

Analyst decisions for detections processed by EP during the time period July-December 1975

Analyst Classification	Number of Processings	Percentage
Accepted as events	3214	49.9
Rejected as being		
- Poor SNR or noise	1258	19.6
- Local events	836	13.0
- Double processings	695	10.8
- Communication errors	433	6.7
Sum Processed	6436	100.00

Table III.2

Number of teleseismic and core phase events reported during the time period July-December 1975

Month	Teleseismic	Core	Sum
Jul 75	450	221	671
Aug	369	158	527
Sep	312	83	395
Oct	346	100	446
Nov	380	84	464
Dec	314	74	388

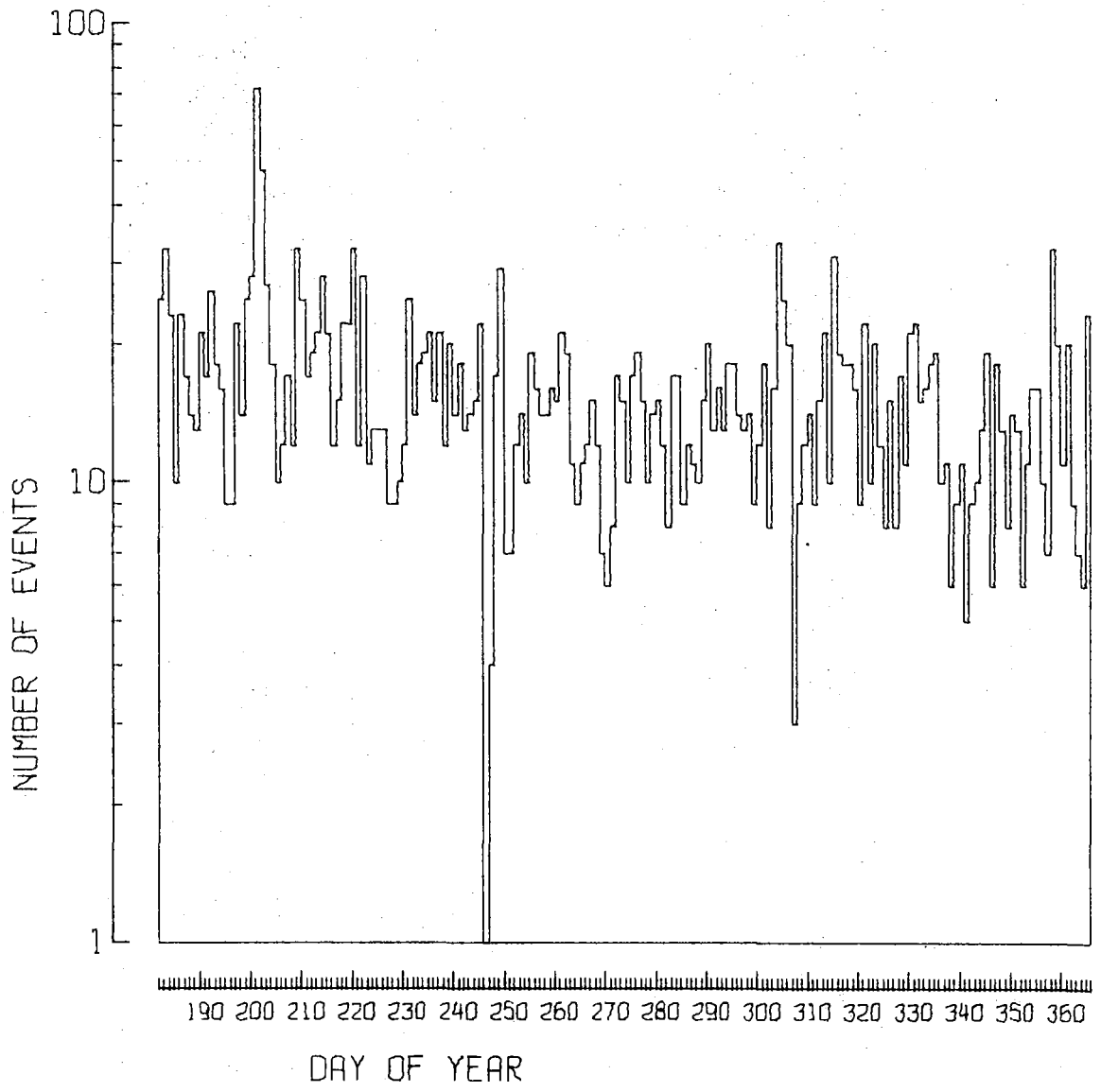

Fig. III.1 Number of events as a function of day of year July - December 1975.

IV IMPROVEMENTS AND MODIFICATIONS

IV.1 Detection Processor

From the end of October the Detection Processor will check the reduced Selected Surveillance detections to see if a detection is from one of a set of beam directions (2, 55, 117 or 126) all related to possible explosion test sites. If a detection is on one of these beams, and has a signal-to-noise ratio above a certain threshold, a 'Possible Explosion' warning message will be printed on the 1052 Console Typewriter as well as on the 1403 Printer, to alert the operator. Also, if the MSTA-value of a Selected Surveillance detection exceeds a certain threshold, a 'Large Event' warning message will be printed on the 1052 Typewriter and the 1403 Printer. Detailed instructions have been worked out and implemented for the operators when these messages occur. The basic procedure is that the Strip Chart Recorder is started with on-line long period data as soon as the message occurs, the event is immediately processed on Fast EP, and a seismologist is called upon in accordance with a certain system of priorities.

IV.2 Event Processor

No modifications were performed in the EP system during this period.

IV.3 Array Instrumentation

The status of a number of improvement projects is as follows:

- Depression of noise in SLEM discrete inputs*	The material needed for modification has been procured and a few modules are ready for field installation.
- Too low surge rating of BE protection cards*	Thirty-one cards are modified and ready for field installation.
- False triggering of CTV water monitor	The "turn-on point" has been adjusted on all subarrays.
- Trends towards negative DC offset in the SP/LTA	Modification (refer Larsen and Nilsen, 1974) is accomplished on the last five subarrays left over from last reporting period.

* Refer Larsen, Falch and Pettersen, 1975.

At 14C the unit installed on channel 05 29 April 1975 dividing the net frequency 18 times to 2.78 Hz with signal amplitude of 9.2 volts peak-to-peak, is still used for investigation purposes.

As of 19 September 1975 14C03 and the 14C LP channels were attenuated -30 dB in order to receive unsaturated seismic signals from events up to M_b 7.0 at a 30 degree distance.

V MAINTENANCE ACTIVITY

This section includes a review of the maintenance accomplished at the subarrays by the field technicians as a result of the remote array monitoring and visual inspections. There are no changes in the monitoring schedule in the period.

Maintenance Visits

Fig. V.1 shows the number of visits to the different subarrays in the period. Excluding visits caused by troubles in the communication system and measurements to verify CCITT M102 line specifications, the subarrays have on the average been visited 4.6 times.

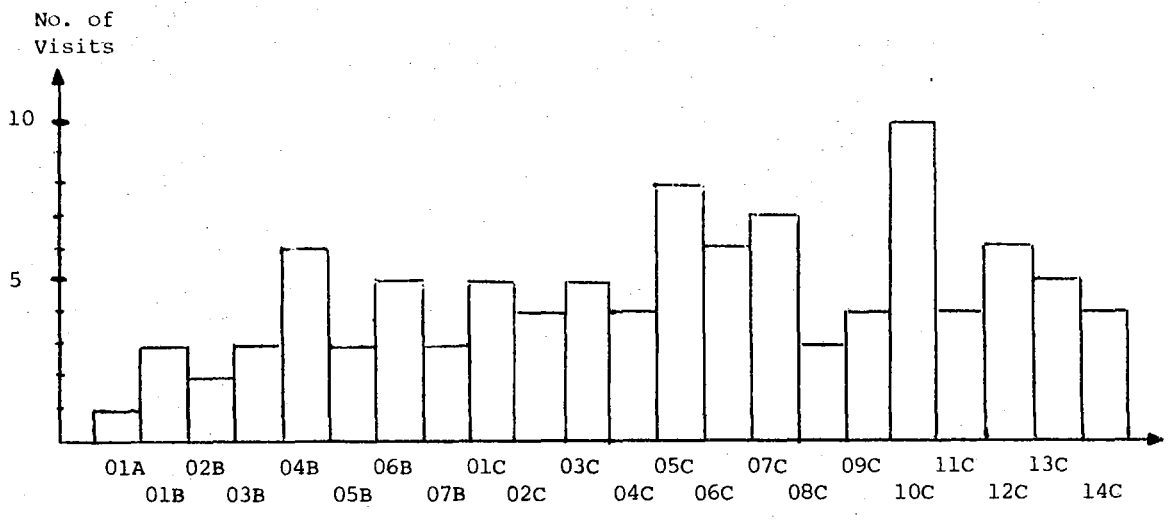

Fig. V.1 Number of maintenance visits to the NORSAR subarrays 1 July 1975 - 31 December 1975.

Preventive Maintenance Projects

The preventive maintenance work in the array is described in Table V.1.

Table V.1

Unit	Action	No. of Channels Acc.	Remain.	Comments
SP Seis.	Adjustment of damping	2		12C04,06
LTA	Adjustment of SP DC offset to pos.bias	49		
	Modification of SP DC offset adjustment range (R12)*	30		04B,01C,08C, 13C,14C
RA-5	Replacement of RA-5's with new batteries to prevent power decay	11		12C01-03,05,06; 14C
CTV	Cleaning of CTV	15 (sub-arrays)		01A,01B,02B, 05B,01C,02C, 04C,06C,07C, 08C,09C,10C, 11C,13C,14C

* Refer Larsen and Nilsen, 1974.

Disclosed Malfunctions on Instrumentation and Electronics

Table V.2 gives the number of accomplished adjustments and replacements of field equipment in the total array with the exception of those mentioned in Table V.1.

Table V.2

Total number of required adjustments and replacements in the NORSAR data channels and SLEM electronics 1 July 1975 - 31 December 1975.

Unit	Characteristic	SP		LP	
		Repl.	Adj.	Repl.	Adj.
Seis-	Damping	1			4
mometer	Nat. Freq.	1			
	Sensitivity		1		
	RCD			11	4
Seis-	Gain	2	4		
mometer	Distortion	4			
Ampli-	Cal.amp.inop.	2			
fier	Balance		2		
(RA-5)	Taper pin block	3	2		
LTA	Ch. gain		17		
	Filter discr.	1			
	DCO		5		
	CMR	1	1		
	Kl relay fault	1			
BE card		40			
WHV Prot. Card		4			
SLEM					
BB gen.		1	4		
RSA/ADC		1			
EPJ			1		

Malfunction of Rectifiers, Power Loss, Cable Breakages

Malfunction of the rectifiers and power loss requiring action of the field technicians or local power company are reported in Table V.3.

Table V.3

Faults disclosed in subarray rectifiers and power loss

Sub-array	Fault	Period of inoperation	Comments
01B	Rectifier trafo M2 burned	14-15 July	
02B	Main AC power break	7-9 Dec	
02C	Rectifier continuous in high charge		Timer defective
03C	Rectifier failed to go into high charge		Timer faulty

Sixteen cable breakages have been repaired in the period requiring 53 days' work of the field technicians. The local power company completed the repair of the power cable to 01C and 1 KV installations (previously 10 KV) 29 August.

Conclusion

The period is characterized by a stable and satisfactory operation of the array instrumentation, resulting in a normal maintenance activity. The number of replaced LP RCDs was eleven during the first three months of the period, in the last three months none have been replaced, thus indicating a more stable trend.

Modification of SP DC offset adjustment range is now completed. The array average DC offset of the SP channels was plus one millivolt at the end of the period.

Also the preventive maintenance program for the WHV's and RA-5's is completed. This program is planned reinitiated in summer 1977.

A number of BE lightning protection cards have been modified for improved surge rating and are ready for field installation. This program is planned completed on most of the subarrays before the next lightning season in summer 1976.

REFERENCES

Larsen, P.W., K. Falch and R. Pettersen (1975): Modification proposals on SLEM and associated equipment, NORSAR Internal Report No. 3-74/75, NTNF/NORSAR, Kjeller, Norway.

Larsen, P., and A. Nilsen (1974): DC offset trim modification of NORSAR short period line terminating amplifier, NORSAR Internal Report No. 8-73/74, NTNF/NORSAR, Kjeller, Norway.

ABBREVIATIONS

AC	-	Alternate Current
ADC	-	Analog-to-Digital Converter
BB	-	Broad Band
BE card	-	Lightning Protection Card
CMR	-	Common Mode Rejection
CTV	-	Central Terminal Vault
DC	-	Direct Current
DCO	-	DC offset
EPU	-	External Power Unit
LP	-	Long Period
LTA	-	Line Terminating Amplifier
RA-5	-	SP Seismometer Amplifier
RCD	-	Remote Centering Device
RSA	-	Range Switching Amplifier
SLEM	-	Seismic Short and Long Period Electronics Module
SP	-	Short Period
WHV	-	Well Head Vault

VI DOCUMENTATION DEVELOPED

VI.1 Reports, Papers

Aki, K., A. Christoffersson and E.S. Husebye: Determination of the three-dimensional seismic structure of the lithosphere, submitted for publication.

Aki, K., A. Christoffersson and E.S. Husebye: Three-dimensional seismic structure of the lithosphere under Montana LASA, Bull. Seism. Soc. Am., in press.

Berteussen, K.A.: The origin of slowness and azimuth anomalies at large arrays, Bull. Seism. Soc. Am., in press.

Berteussen, K.A.: Array analysis of lateral inhomogeneities in the deep mantle, Earth Plan. Sci. Lett., 28, 212-216, 1975.

Berteussen, K.A. (ed.): Final Technical Report NORSAR Phase 3, 1 July 1974 - 30 June 1975.

Bungum, H., and E.S. Husebye: The seismicity of Fennoscandia, Proceedings, ESC Symposium on Earthquake Risk for Nuclear Power Plants, in press.

Bungum, H., and D. Tjøstheim: Discrimination between Eurasian earthquakes and underground explosions using the m_b:M_s method and short period autoregressive parameters, Geophys. J.R. astr. Soc., in press.

Haddon, R.A.W., E.S. Husebye and D.W. King: Origins of precursors to P'P', Phys. Earth Plan. Int., in press.

Husebye, E.S., A. Christoffersson, K. Aki and C. Powell: Preliminary results on the 3-dimensional seismic structure of the lithosphere under the USGS Central California Seismic Array, submitted for publication.

Husebye, E.S., D.W. King and R.A.W. Haddon: Precursors to PKIKP and seismic wave scattering near the mantle-core boundary, J. Geophys. Res., in press.

King, D.W., and G. Calcagnile: P-wave velocities in the upper mantle beneath Fennoscandia and Western Russia, Geophys. J.R. astr. Soc., in press.

King, D.W., E.S. Husebye and R.A.W. Haddon: Processing of seismic precursor data, Phys. Earth Plan. Int., in press.

Ringdal, F.: Maximum likelihood estimation and seismic magnitude Bull. Seism. Soc. Am., in press.

Tjøstheim, D.: Recognition of waveforms using autoregressive feature extraction, Correspondence IEEE Trans. Computers, submitted for publication.

Tjøstheim, D.: Spectral representation and density operators for infinite-dimensional homogeneous random fields, Wahrscheinlichkeitsteorie und verwandte gebiete, submitted for publication.

VI.2 Program Documentation

The following programs have been developed at NORSAR during the reporting period:

- A new improved magnetic tape read routine that will allow the programmer to build decisions into his program about how to deal with data checks, etc. (N/PD-82, READTA)
- An improved version of the HYPERMAP map program, allowing more detailed mapping in 11 different projections, for all or parts of the world (N/PD-83, SUPERMAP)
- A program that calculates long periodic beam power as function of azimuth, slowness and time (N/PD-84, LPBEAM)
- A program that calculates a long periodic array beam, as well as uncorrected and response corrected power spectra for individual channels and the beam (N/PD-85, LPBMSP)
- A program performing a frequency-time analysis of a given time series, by means of multiple narrow band filtering in the frequency domain (N/PD-86, FTAN)
- A program for plotting individual short period traces from the HR-tape, with trace spacing proportional to the projection of the individual instrument locations onto the arrival azimuth (N/PD-87, SPSECT)
- A general purpose subroutine for plotting contours of a two dimensional scalar field, represented as a two-dimensional grid of N by M observations (N/PD-88, CPLOT)
- A routine giving back the number of characters plotted when using the NUMBER plotting subroutine (N/PD-89, NUMCAR).

In addition, various other programs have been either developed at NORSAR, or received from other sources and modified for use here.

VII SUMMARY OF SPECIAL AND TECHNICAL REPORTS/ PAPERS PREPARED

VII.1 P-wave Velocities in the Upper Mantle beneath Fennoscandia and Western Russia

A detailed and extensive record section which has been constructed from recordings at NORSAR of presumed explosions in continental Russia exhibits two distinct (T,Δ) triplications. A particularly noteworthy feature of the (T,Δ) curves defined by the record section is the pronounced extension of the first-arrival branch for $\Delta \lesssim 21^{\circ}$ as a secondary arrival to a distance $\Delta \sim 33^{\circ}$. The reliable identification of these upper mantle travel-time branches has been possible because of the extremely dense, areal sampling of the NORSAR configuration.

The details of the P-wave multibranching offer powerful constraints on the nature of the upper mantle transition zone beneath the Baltic Shield and Russian platform. Notwithstanding the questions of uniqueness and baseline uncertainty, the following features appear to be demanded by the observational data:

1. A relatively small positive velocity gradient below the Moho to about 420 km depth
2. A relatively rapid increase in velocity by about 7% near 420 km depth
3. A relatively rapid increase in velocity by about 4% near 690 km depth
4. A relatively large positive gradient between the 'discontinuities' near 420 and 690 km depth.

A simple representative velocity model KCA has been derived which accounts adequately for all the principal features of the observational data. In the interests of simplicity, the model KCA includes first order discontinuities in preference to the depth-distributed discontinuities of comparable effect. The KCA model and the associated reduced (T,Δ) curves are shown in Fig. VII.1.1. It is apparent in this figure that the differences in the model and inferred observational

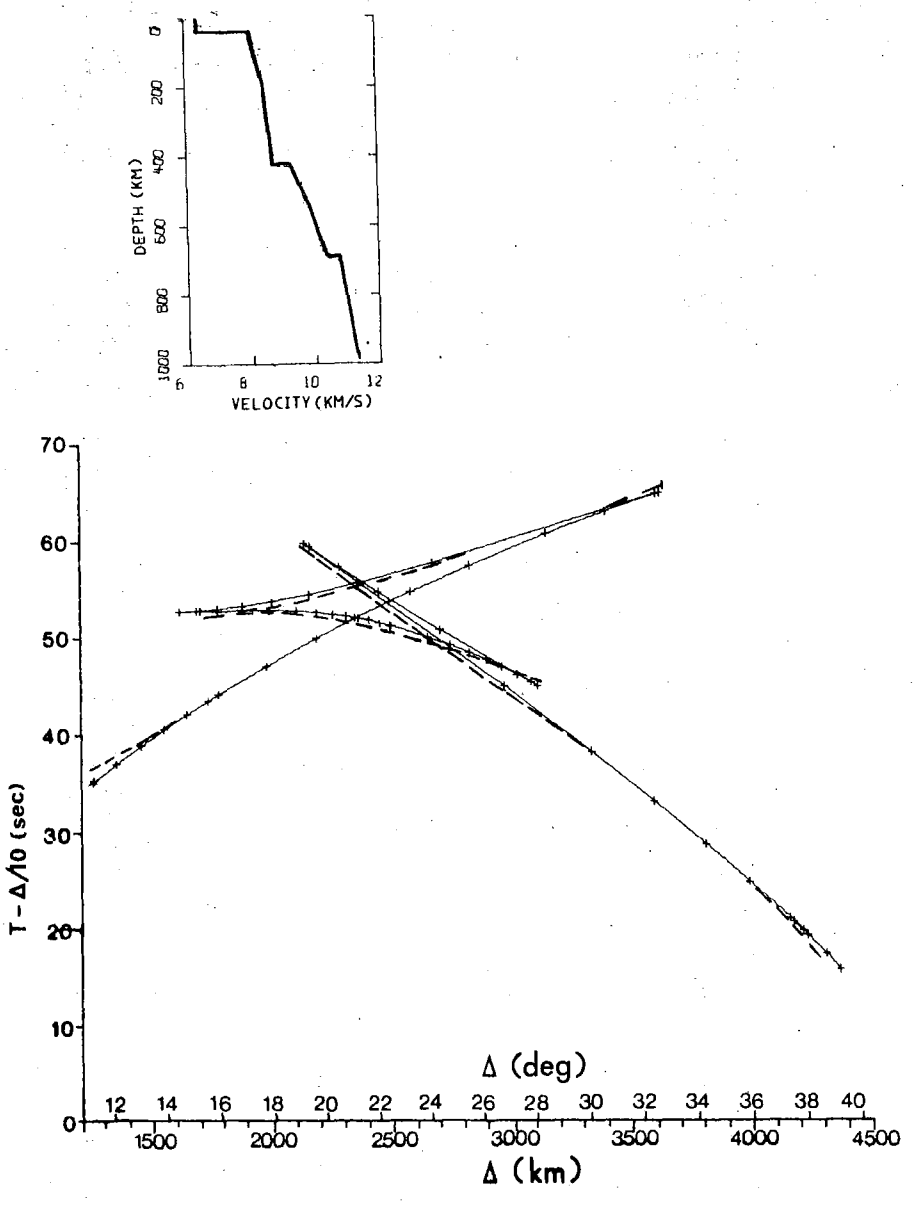

Fig. VII.1.1 P velocity model KCA, and corresponding reduced travel time-distance curves (full lines). Differences in the observed and model reduced times are shown by dashed lines. The spacing of the +'s on the model (T,Δ) curves is proportional to $d^2T/d\Delta^2$ and is indicative of relative amplitudes (considering geometrical spreading only).

(T,Δ) curves are minor. In addition, the KCA model is broadly consistent with observed relative amplitudes of the various branches, although in this respect the uncertainties are, of course, relatively large because of possible departures from perfect elasticity and other effects.

The discussion by Simpson et al (1974) on the implications of certain velocity models on the composition and state of the upper mantle is fully applicable with regard to the KCA model.

D.W. King
G. Calganile (Bari, Italy)

REFERENCES

Simpson, D.W., R.F. Mereu and D.W. King (1974): An array study of P-wave velocities in the upper mantle transition zone beneath northeastern Australia, Bull. Seism. Soc. Am., 64, 6, 1751-1788.

VII.2 Determination of the 3-dimensional Seismic Structure of the Lithosphere under Montana LASA and under the USGS Central California Seismic Array

The novel 3-dimensional earth-modelling technique presented by Aki, Christoffersson and Husebye (1976) has been used for detailed investigations of the seismic structures beneath the LASA and Central California arrays. The characteristic feature of the above technique is flexibility in modelling the lithosphere. The starting point is the layered medium of classic seismology but each layer is divided into many blocks and assigned a parameter to each block which describes the velocity perturbation from the average for the layer. The data used are teleseismic travel time residuals observed at the LASA array in Montana and USGS Central California array. By isolating various sources of errors and biases, we arrive at a system of equations to determine the model parameters, i.e., the velocity perturbations within the individual blocks. The final solutions were obtained by the use of the generalized inverse and stochastic methods including analysis of resolution and errors of the estimated parameters.

A. The lithosphere beneath LASA

The seismic velocity structure beneath LASA has intrigued seismologists ever since this large aperture array was established in Montana in 1965. A commonly adapted model here is one where material properties within layers are homogeneous but in which the crust thickens sharply from approx. 50 km to approx. 60 km towards northwest near the center of the array. Our results, (Aki et al, 1976) a 3-dimensional seismic image of the lithosphere, are displayed in Figs. VII.2.1 and VII.2.2 in the form of two cross-sections for both the stochastic inverse and generalized inverse solutions respectively.

The most conspicuous feature of the seismic structure under LASA is a low velocity anomaly in the central and NE part of the array siting area with a N60^{o}E trend and persisting from the upper crust to depths greater than 100 km. We are tempted to associate this low velocity zone with wrench faulting and shearing during the Nevadan and Laramide orogenies. The sharp change in crustal thickness proposed in earlier studies is likely to be significantly overestimated because the upper crust and the lower lithosphere appear to share the same anomaly pattern as the proposed Moho topography.

B. The lithosphere beneath Central California - San Andreas fault

We have also studied the seismic structure of the lithosphere beneath central California using data from the 26 U.S. Geological Survey stations which are shown in Fig. VII.2.3 together with the major tectonic features of the area (Husebye et al, 1976).

The San Andreas fault system is a part of the present boundary between the North American and Pacific plates and expresses their relative motions as a transform fault. Between 29 and 21 m.y. the Farallon plate broke up between the Mendocino and Murray fracture zones and the small pieces under-thrust the west coast of North America (Fig. VII.2.4). The Pacific Ocean floor, which came in contact with the North American plate 10-20 m.y. ago, was very young so that the lithosphere was weak and susceptible to deformation. As the eastern margin of the Pacific lithosphere cooled, thickened and grew stronger, it probably became strong enough to bite off a piece of California from North America.

With this background information, let us look at our results for discussion. We start with Layer 1 or the crust with an assumed thickness of 25 km. The trends in the velocity anomalies in Layer 1 (Fig. VII.2.5) run nearly parallel to the direction of the major fault lines in the area; high

velocity to the west of the fault zone and low velocity to the east. The maximum velocity contrast between the two sides for both solutions is around 10%, which is generally consistent with seismic profiling results on velocity differences between the granitic rocks of the Gabilan Range and the Franciscan rocks of the Diablo Range. We also notice that the velocity variation across the fault becomes gradual where the San Andreas fault system branches and sharpens where the faults merge to a narrow zone near Hollister.

The slowness anomalies in Layer 2 (25-50 km) directly beneath Moho are shown in Fig. VII.2.6 for the generalized inverse solution which is different from the stochastic inverse solution. Because of the difference in the two solutions, we shall refrain from any serious attempt to interpret Layer 2 anomalies, but if the general trend in the generalized inverse solution is correct, we find high velocity on the east and low velocity on the west side of the fault, a reversed picture as compared to Layer 1.

The slowness anomalies for Layer 3 (50-75 km) are given in Fig. VII.2.7 showing a definite trend parallel to the fault zone. Just like Layer 1, Layer 3 has high velocity to the west of the fault zone, and low velocity to the east. The remarkable correlation of velocity anomalies in Layers 1 through 3 with the San Andreas suggests that the fault zone penetrates to a depth of at least 75 km.

The slowness anomaly patterns for Layer 4 (75-100 km) and Layer 5 (100-125 km) no longer correlate clearly with the fault zone, as shown in Figs. VII.2.8 and VII.2.9. The similarity of their patterns to Layer 3 is only retained in the northern part of the area, where the velocity is still high to the west and low to the east. This suggests that these layers may not belong to the lithosphere, which is

consistent with the average thickness of the lithosphere of around 80 km in the western United States as obtained by Lee and Solomon (1975) from surface wave attenuation data.

One of the most interesting aspects of the 3-dimensional velocity anomalies is the possibility that the shape of the anomaly may indicate the past or present mode of stress in the lithosphere. We see an indication of a sheared structure in the velocity anomaly pattern along the NW-SE profile in the Pacific plate west of the San Andreas fault. It is expressed in a north-westward migration of a high velocity anomaly along the Pacific coast with increasing depth. The pattern is clearer in the stochastic inverse than in the generalized inverse solution. The direction of shear implied by this pattern may support the hypothesis that the convection current in the asthenosphere is driving the plate motion. We cannot, however, forward a definitive answer to this problem because the profile runs through the peripheral region where the resolution is poor in the stochastic inverse solution and the random error effect is strong in the generalized inverse solution. Additional data currently being collected will hopefully give more definitive results.

Synopsis prepared by E.S. Husebye.

K. Aki (M.I.T., Cambridge, Mass.)
A. Christoffersson (Uppsala)
E.S. Husebye

REFERENCES

Aki, K., A. Christoffersson and E.S. Husebye (1976): Determination of the three-dimensional seismic structure of the lithosphere, J. Geophys. Res., in press.

Aki, K., A. Christoffersson and E.S. Husebye (1976b): Three-dimensional seismic structure of the lithosphere under Montana LASA, Bull. Seism. Soc. Am., in press.

Husebye, E.S., A. Christoffersson, K. Aki and C. Powell (1976): Preliminary results on the 3-dimensional seismic structure of the lithosphere under the USGS Central California Seismic Array, submitted to Geophys. J. R. Astr. Soc.

Lee, W.B., and S.C. Solomon (1975): Inversion schemes for surface wave attentuation and Q in the crust and the mantle, Geophys. J.R. Astr. Soc., in press.

Solomon, S.C., and R.G. Butler (1974): Prospecting for dead slabs, Earth Plan. Sci. Lett., 21, 421-430, 1974.

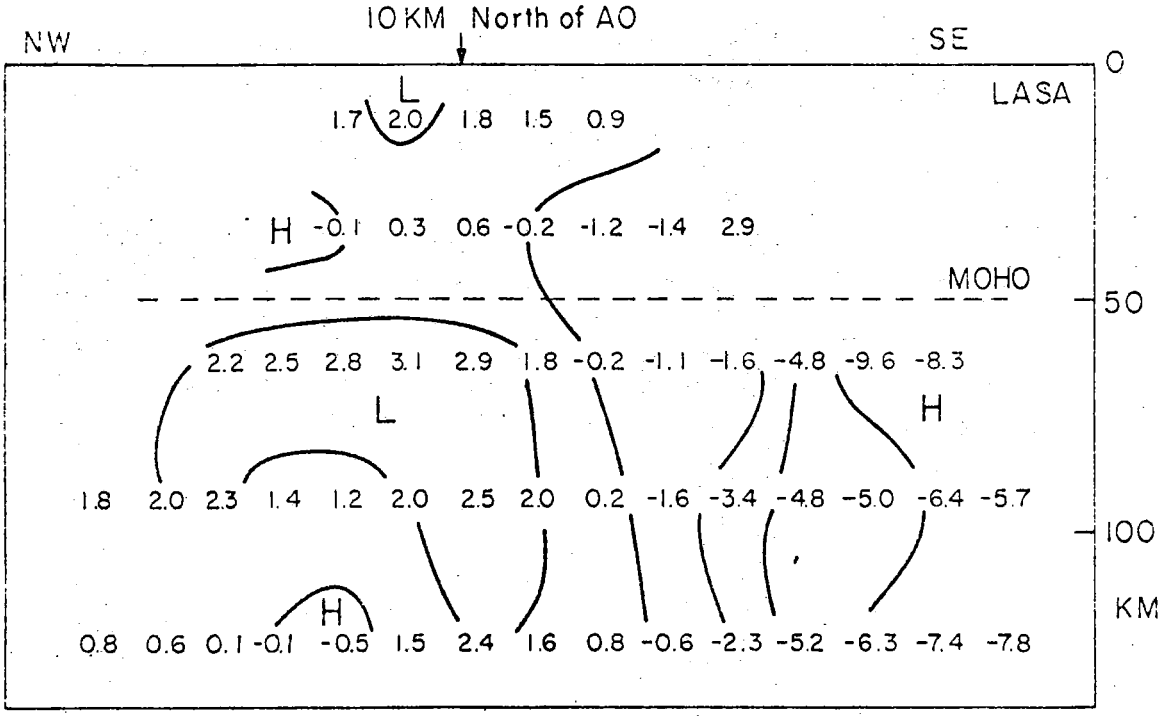

Fig. VII.2.1 Generalized inverse solution for a vertical cross section of the LASA array. The numbers show the fractional velocity perturbation in per cent of the average layer velocity. The letters H and L refer to high and low velocity anomalies.

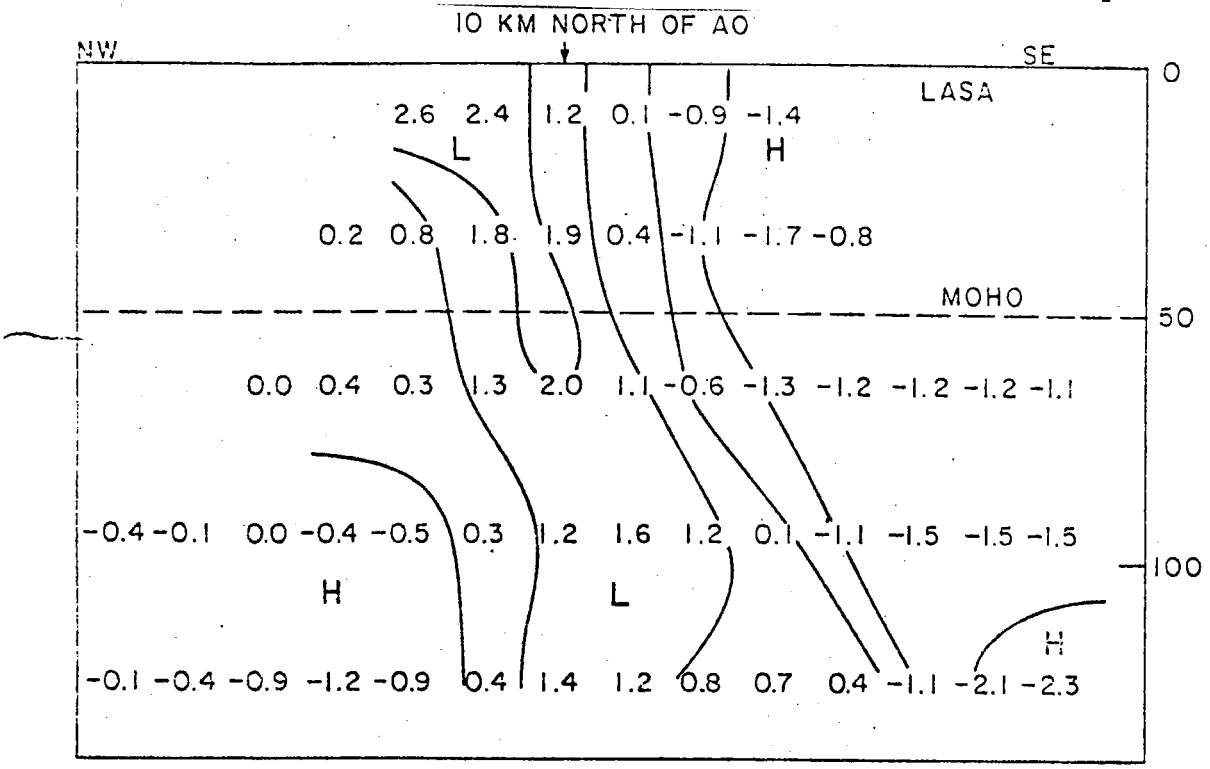

Fig. VII.2.2 Same as in Fig. VII.2.1 for the stochastic inverse solution.

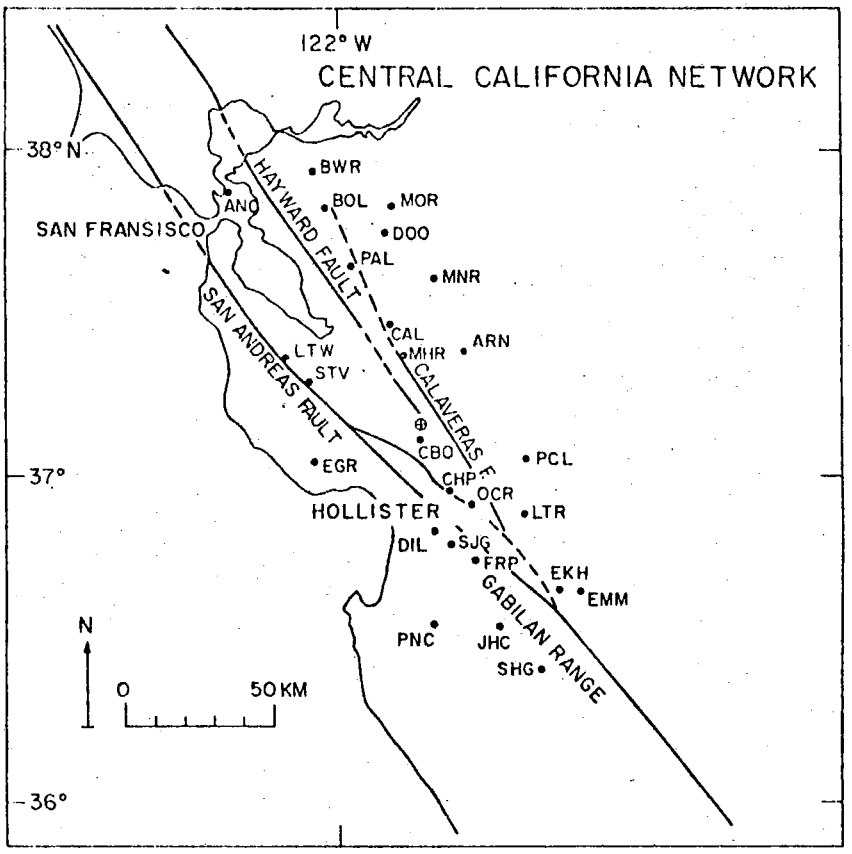

Fig. VII.2.3 U.S. Geological Survey Central California Seismograph stations used in the present analysis.

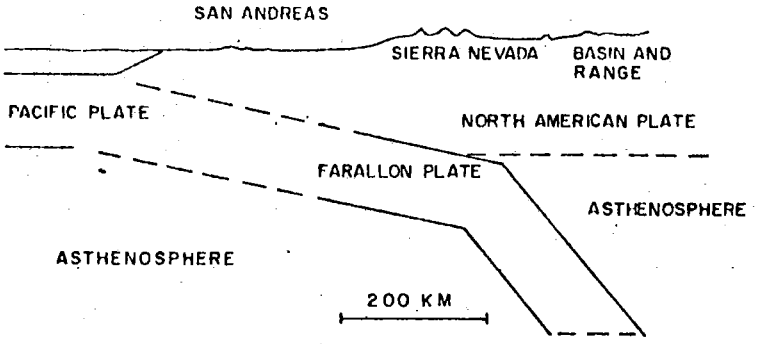

Fig. VII.2.4 A schematic cross-section of hypothetical plate boundaries reproduced from Solomon and Butler (1974).

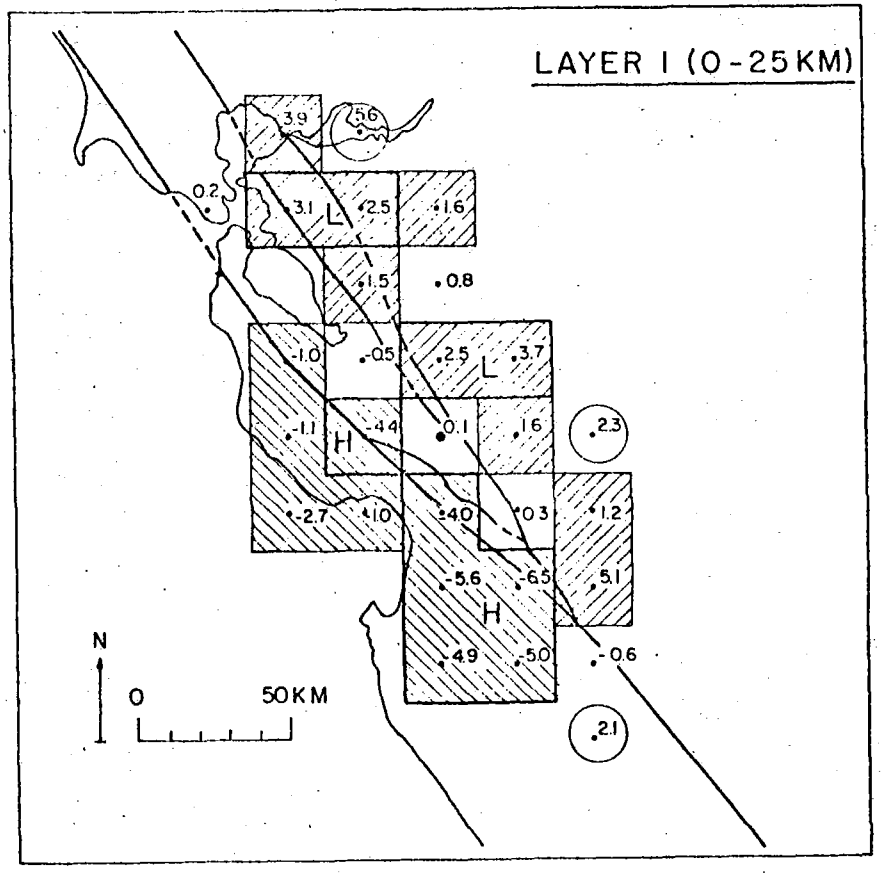

Fig. VII.2.5 Generalized inverse solution for Layer 1. The numbers show the fractional slowness perturbation in per cent of the average layer slowness. The heavy shaded areas correspond to the magnitude of solution greater than twice the standard error. The letters L and H refer to low and high velocity anomalies respectively. Blocks not properly resolved are encircled. The network center is marked by a larger solid circle.

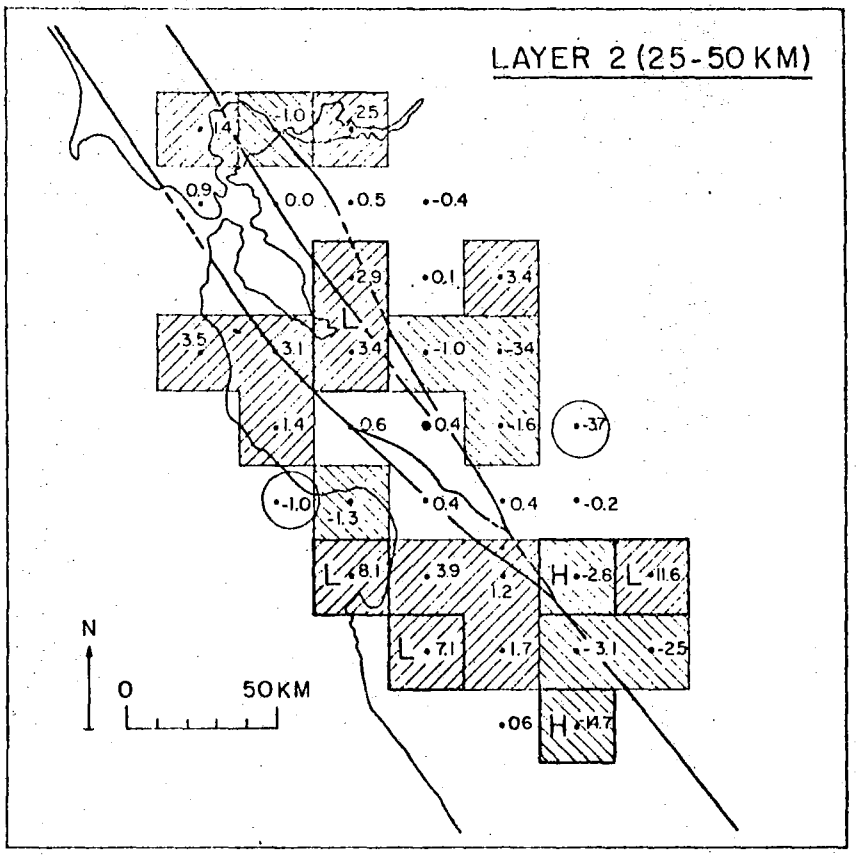

Fig. VII.2.6 Generalized inverse solution for Layer 2. See Fig. VII.2.5 for explanation of symbols.

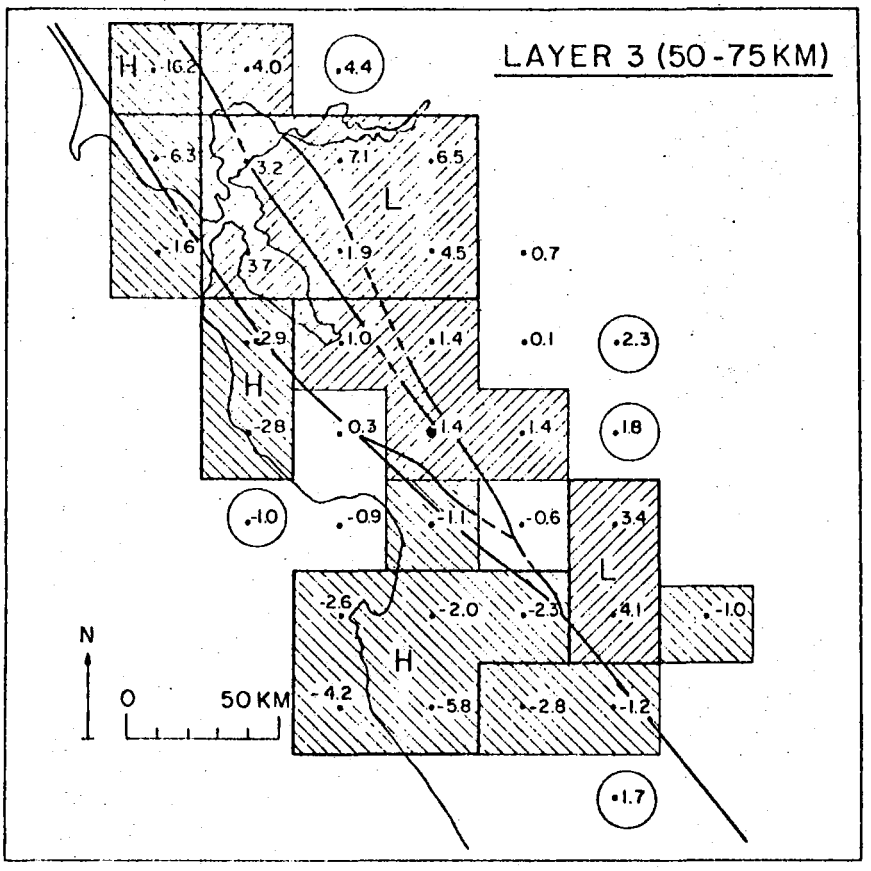

Fig. VII.2.7 Generalized inverse solution for Layer 3. See Fig. VII.2.5 for explanation of symbols.

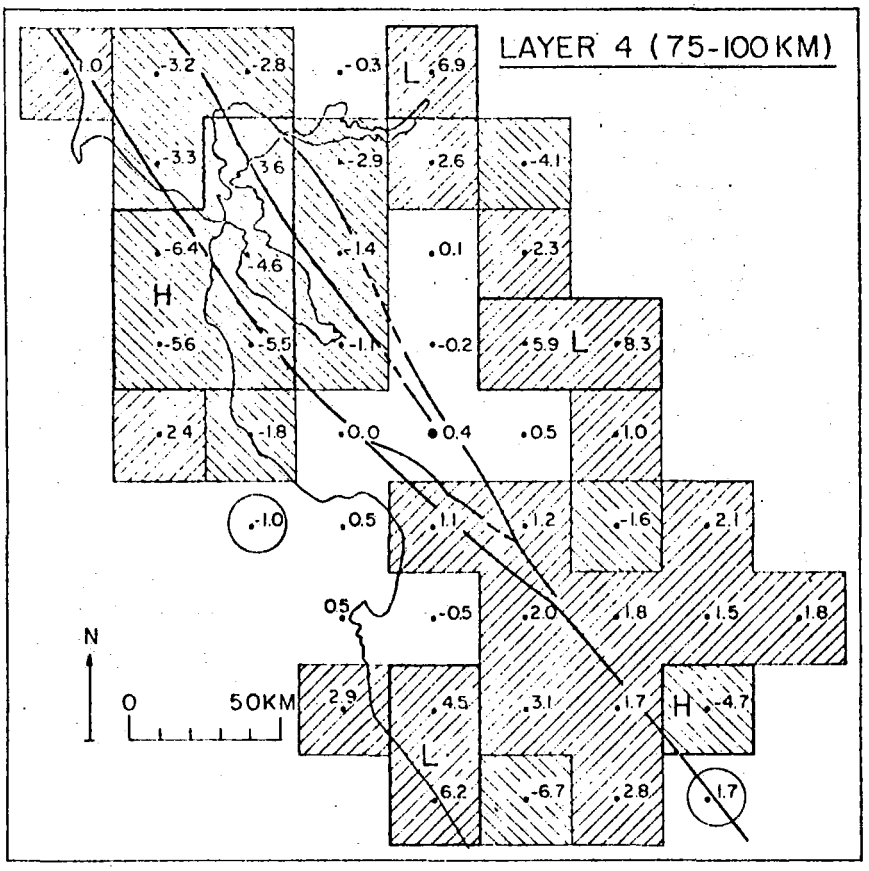

Fig. VII.2.8 Generalized inverse solution for Layer 4. See Fig. VII.2.5 for explanation of symbols.

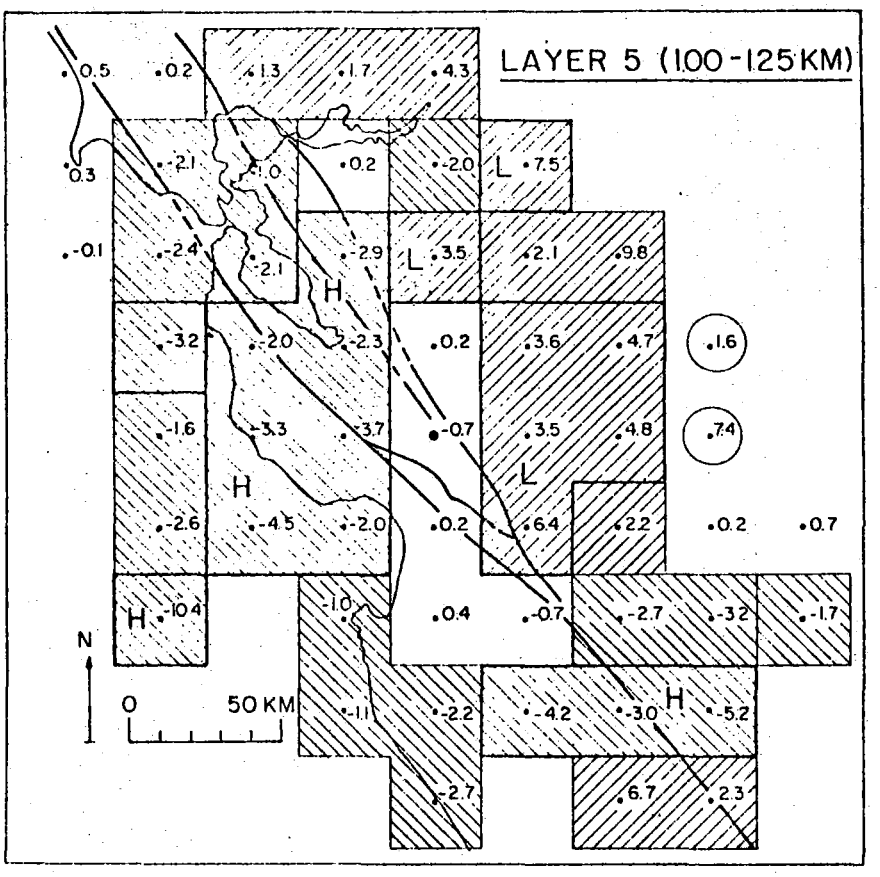

Fig. VII.2.9 Generalized inverse solution for Layer 5. See Fig. VII.2.5 for explanation of symbols.

VII.3 Origins of Precursors to P'P'

Observed precursors to the seismic phase P'P' consist of trains of waves arriving up to about 150 seconds before the main P'P' phases. Until recently these precursors have usually been interpreted as 'P'dP' waves' resulting from reflections of PKP waves from the undersides of postulated horizons at various depths d below the Earth's surface in regions where the associated P'P' reflections occur. The earliest such P'dP' arrivals consistently observed correspond to a reflecting horizon at a depth of about 650 km and so these precursors are designated P'650P'. In this particular case the evidence supporting the P'dP' interpretation, including evidence obtained in the present study, is extremely strong. For many of the precursor arrivals following P'650P', however, the P'dP' interpretation is questionable.

Seismic scattering in the lowest 200 km of the mantle (region D") has previously been shown to account for observed precursors to PKIKP (Haddon and Cleary, 1974; King et al, 1973; Husebye et al, 1976) while scattering in the crust and upper mantle has been shown to account for observed precursors to PP (King et al, 1975). Since P'P' waves are simply PKP waves which have undergone reflection at the earth's free surface, scattering effects similar to those associated with PKP and PP are also to be expected for P'P'.

The consequences of postulating irregularities in layers at the top and bottom of the mantle are examined theoretically in respect of scattering associated with the usual P'P' phases. The theoretical results obtained are then compared with detailed observational evidence on P'P' precursor wavetrains starting up to 50 seconds prior to the main P'P' phases recorded at the NORSAR array.

The analysis procedure adopted for investigating P'P' precursor wavetrains, called **BEAMAN** analysis, has been described in an earlier report (see also King et al, 1975). Some typical examples of the power diagrams obtained by the **BEAMAN** procedure are shown in Fig. VII.3.1. The numbers 1, 2, 3,... on the contours in each figure specify the power in dB below the reference level for the particular time interval to which the diagram belongs. Note the good agreement between the locations of the observed maximum power peaks and the theoretical results.

The hypothesis of seismic scattering by small-scale random inhomogeneities in the uppermost few hundred km of the mantle (in and near the crust) and in the lowermost few hundred km of the mantle (region D") is shown to be consistent with detailed observational data on precursors to P'P' recorded at the NORSAR seismic array for arrival times 0 to 50 seconds before P'P'(BC). The data are generally inconsistent with theoretical results for the P'dP' interpretation in this time interval. The NORSAR data appear to be quite characteristic of similar but less detailed data on precursors to P'P' obtained by other authors, previously interpreted as indicating the presence of a number of sharp reflecting discontinuities in the uppermost 200 km of the mantle below the crust. The scattering interpretation removes any need for postulating such discontinuities in this region.

R.A.W. Haddon
E.S. Husebye
D.W. King

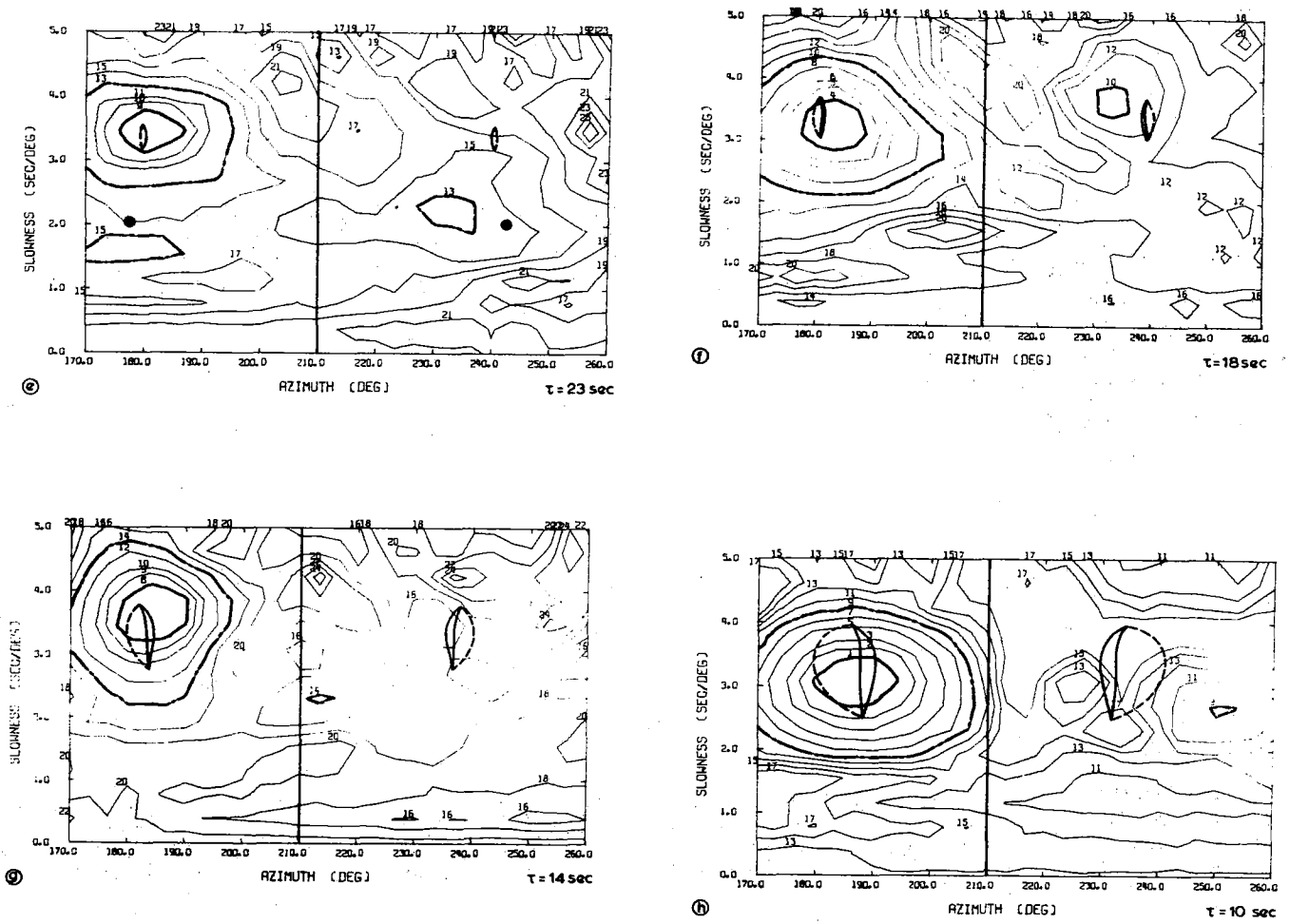

Fig. VII.3.1 Examples of contoured beam power levels in slowness-azimuth space (BEAMAN diagrams) for 2-second intervals of the P'P' precursor wavetrain for lead times τ before the theoretical arrival time of P'P'(BC). The contours represent power levels in dB below relative power maxima of 23.9 dB (frame e), 26.2 dB (frames f to j) and 27.1 dB (frames k and l). Contours enclosing significant peaks in each frame are thickened and theoretical slowness-azimuth ranges for scattered waves for the same arrival time are plotted in each frame centred on the calculated NOAA azimuth. Note the good agreement between the locations of the observed maximum power peaks and the theoretical results.

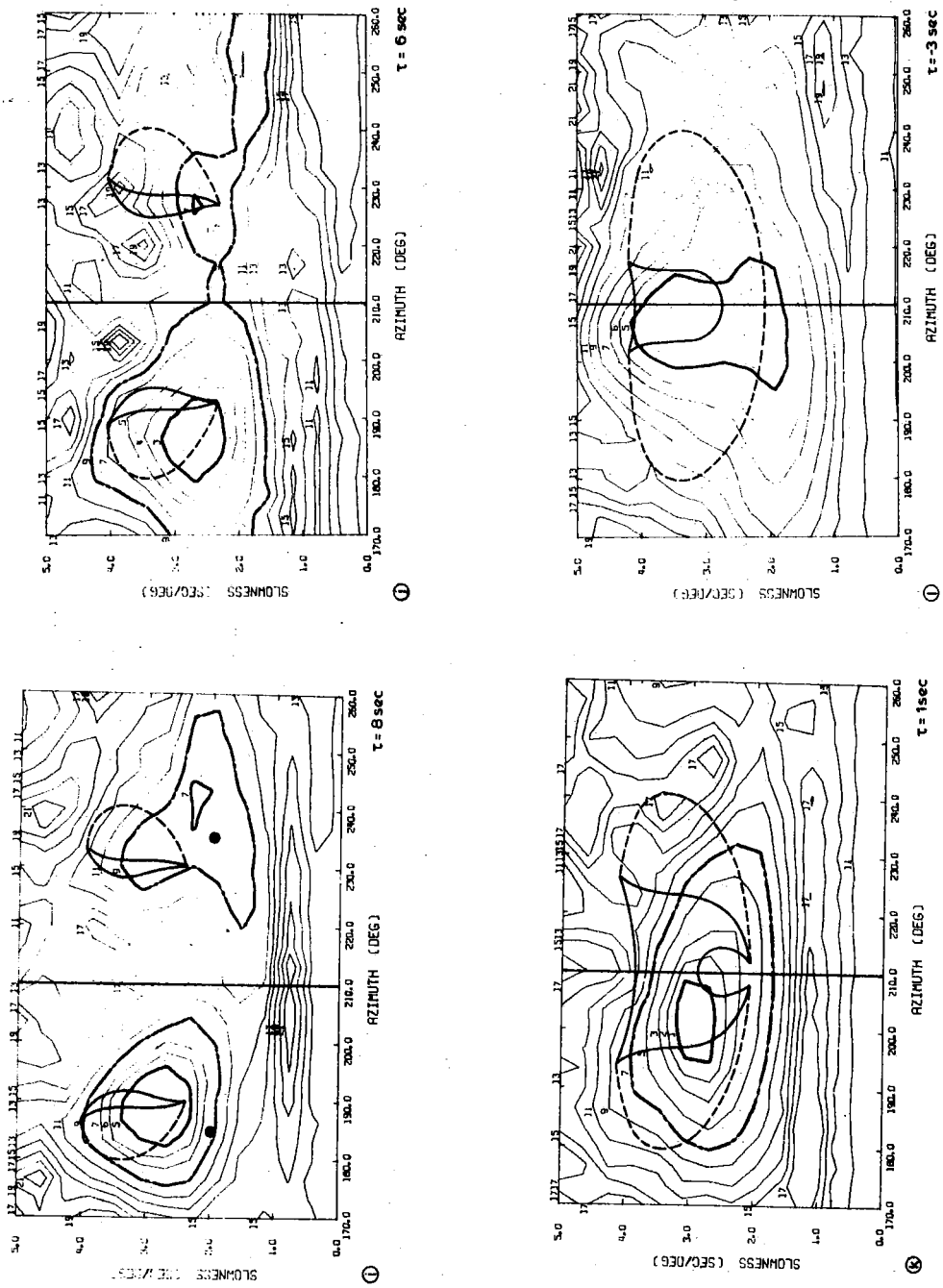

Fig. VII:3.1 (cont.)

REFERENCES

Haddon, R.A.W., and J.R. Cleary (1974): Evidence for scattering of seismic PKP waves near the mantle core boundary, Phys. Earth Planet. Int., 8, 211-234.

Husebye, E.S., D.W. King and R.A.W. Haddon (1976): Precursors to PKIKP and seismic scattering near the mantle-core boundary (to appear in Geophys. J.R. astr. Soc.).

King, D.W., R.A.W. Haddon and J.R. Cleary (1973): Evidence for seismic scattering in the D" layer, Earth Planet. Sci. Lett., 20, 353-356.

King, D.W., R.A.W. Haddon and E.S. Husebye (1975): Precursors to PP, Phys. Earth Planet. Int., 10, 103-127.

VII.4 An Analysis of Rayleigh Waves from Novaya-Zemlya Explosions

The Russian test sites on Novaya-Zemlya are located in the middle of the island (azimuth $\approx 35^{o}$ at NORSAR) and on the southern end of it (azimuth $\approx 42^{o}$). NORSAR has recordings with strong Rayleigh waves of 6 events from the northern test site and 3 from the southern. For all these events a beam made of the 22 long period vertical instrument recordings has been analyzed for dispersion characteristics. The analysis is done by means of multiple narrow band filtering in the frequency domain. The main output of the program is a map of power distribution in the frequency time domain. Fig. VII.4.1 shows such a map for an event in the northern test site. The thick line on the figure connects points of maximum energy. The most notable effect on the figure is the low group velocity observed, say around 2.5 km/sec for waves with period less than 20 seconds. On Fig. VII.4.2 is then shown the same type of figure for an event from the southern test site, and a much more complicated pattern arises. First it is noted that for waves with period less than 20 seconds the main (first) arrival now has a group velocity of approximately 2.9 km/sec. Secondly it is noted that two later arrivals may be observed with group velocity 2.5 km/sec and 2.2 km/sec respectively. Checking the azimuth for the different arrivals (this has been done both with an ordinary time domain beam power program and with a high resolution program), it is found that the event on Fig. VII.4.1 has an azimuth close to the correct one. For the data on Fig. VII.4.2, the first and third arrivals have an azimuth close to the correct one for this event, while the second arrival has an azimuth which is roughly the same as that for the event on Fig. VII.4.1. These preliminary studies indicate that the extremely low group velocities observed for events from the northern test site are caused by thick sediment layers in the Barents Sea on this path, while the southern path has somewhat thinner sediment layers. The multipathing (arrival 2 and 3 on Fig. VII.4.2) is believed to be caused by discontinuities within the Barents Sea, the details of these will be studied further.

A.L. Levshin (Moscow)
K.A. Berteussen

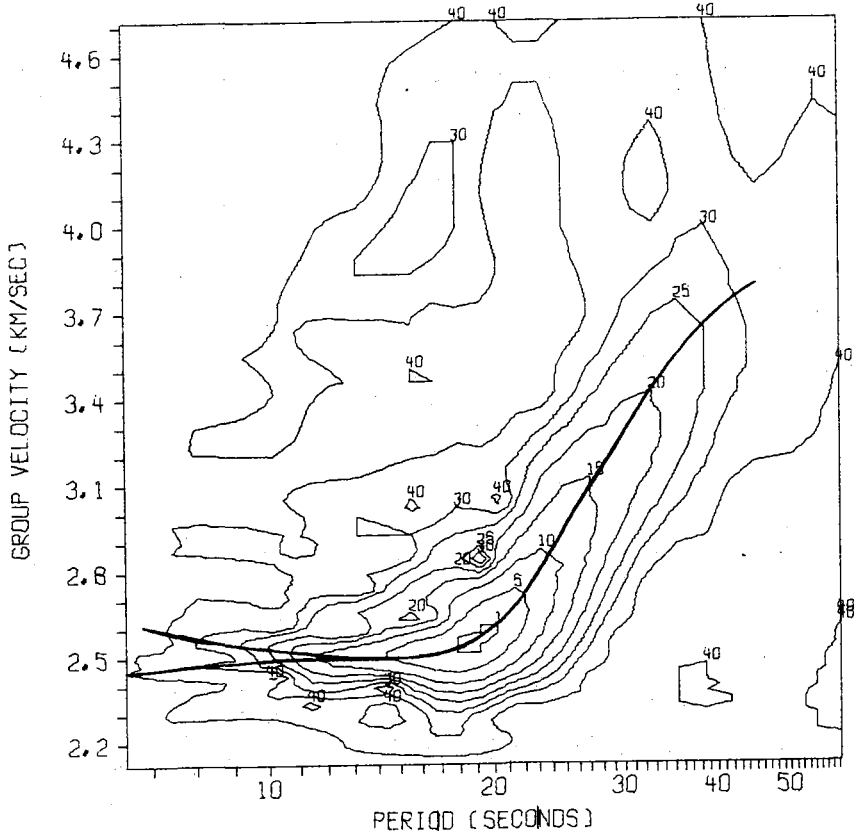

Fig. VII.4.1 Power as a function of group velocity and period for Novaya-Zemlya event of August 29, 1973. Distance=20°, Azimuth=35°. The thick line connects points of maximum energy.

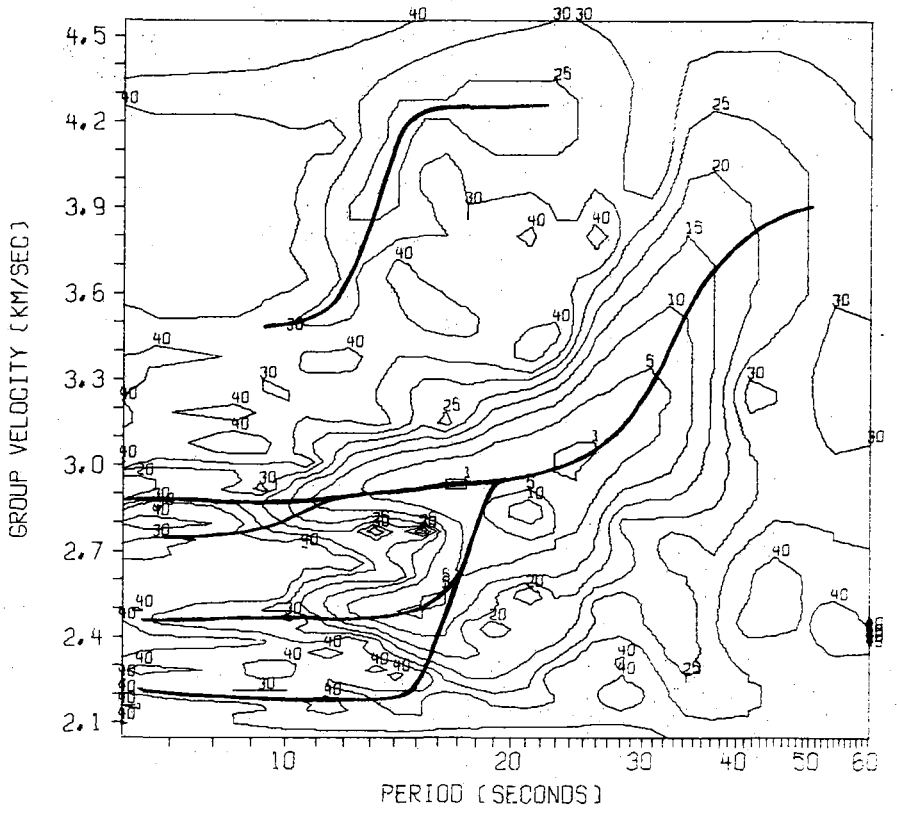

Fig. VII.4.2 Same as Fig. VII.4.1 for Novaya-Zemlya event of October 27, 1973. Distance=20°, Azimuth=35°.

VII.5 NORSAR Operational Capabilities

Using the same regionalization and estimation procedures as Bungum and Husebye (1974) an evaluation of the NORSAR Event Processor performance for the period April 1972 until March 1975 has been undertaken.

Detectability Thresholds

Table VII.5.1 shows the estimated 50 and 90 per cent cumulative detection thresholds for the period April 1972 - March 1973, April 1973 - March 1974, April 1974 - March 1975 and April 1973 - March 1975. There is a small tendency for higher thresholds for the last two years, although for regions 6, 7 and 8 the thresholds for the period 1974-75 are lower than those for 1972-73. The main impression is that there is a remarkable stability in the performance over the three years. Using only one year intervals, there are some regions where there are too few events, or the distribution is such that the method applied is not usable. With three years of data a relatively reliable estimate of the detection threshold for all the regions is, however, achieved.

Location Estimation

The difference in epicenter solutions has been calculated for the events reported jointly by USGS and NORSAR in the period January 1973 until March 1975. Fig. VII.5.1 presents the results for region 14 (distance limits 30-90 degrees from NORSAR) in increments of 50 km location difference. Fig. VII.5.2 shows the same data for the interval February to November 1972. It is seen that the distribution in Fig.VII .5.1 has a much shorter tail, indicating that most of the large location errors have been removed. Since the data is so skew the 50 per cent (median) and the 90 per cent level of location differences is used as characterizing parameters. In Table VII.5.2 the values observed for the period February to November

1972 (by Bungum and Husebye, 1974) is listed together with the values observed for the period January 1973 until March 1975. For most of the regions there is a considerable reduction in location differences especially on the 90 per cent level. This is partly due to the implementation of new region corrections at NORSAR in November 1972, and partly due to the more experienced analysts.

A more thorough discussion of both detection and location performance will be published in a forthcoming report.

K.A. Berteussen
H. Bungum

REFERENCES

Bungum, H., and E.S. Husebye (1974): Analysis of the operational capabilities for detection and location of seismic events at NORSAR, Bull. Seism. Soc. Am., 64, 637-656.

Table VII.5.1

Cumulative 50 and 90 per cent detection thresholds in terms of NORSAR m_b units for the intervals April 1972 - March 1973, April 1973 - March 1974, April 1974 - March 1975 and April 1972 - March 1975. N means number of events. A dash indicates that there were too few data or a too difficult distribution for detectability estimates. Area of coverage for the different regions is given in Table VII.5.2. (They are defined in Bungum and Husebye, 1974.)

REGION	1972 - 1973			1973 - 1974			1974 - 1975			1972 - 1975		
	MB-50	MB-90	N	MB-50	MB-90	N	MB-50	MB-90	N	MB-50	MB-90	N
1	-	3.6	392	3.4	3.8	319	3.6	3.8	397	3.4	3.7	1108
2	-	-	99	3.5	4.0	91	-	-	42	2.7	3.8	232
3	3.7	4.1	138	3.9	4.4	88	3.8	4.3	102	3.8	4.3	328
4	-	-	147	3.5	3.9	151	3.4	3.8	184	3.4	3.8	482
5	3.0	3.6	466	3.6	3.7	409	3.3	3.8	469	3.1	3.6	1344
6	3.4	3.8	386	3.3	3.8	241	3.1	3.5	263	3.3	3.8	890
7	3.2	3.6	524	3.1	3.5	396	3.1	3.5	770	3.1	3.5	1690
8	-	4.4	299	3.0	4.0	290	3.3	3.7	453	3.2	3.6	1042
9	4.0	4.5	961	3.9	4.5	546	3.9	4.4	466	3.9	4.5	1973
10	3.4	3.9	841	3.3	3.7	1395	3.4	3.9	912	3.4	3.8	3148
11	4.0	4.6	146	4.3	4.6	238	4.2	4.7	141	4.1	4.5	525
12	3.4	3.9	663	3.3	3.9	777	3.4	4.0	799	3.4	3.9	2239
13	4.4	4.7	88	4.2	4.9	91	4.4	4.9	165	4.3	4.8	344
14	3.4	3.8	4335	3.4	3.9	4011	3.5	3.9	4278	3.4	3.9	12624
15	4.0	4.5	1057	4.2	4.6	1298	4.3	4.7	1188	4.2	4.6	3543

Table VII.5.2

Estimates of median and 90 per cent location difference (in km) between USGS and NORSAR epicenter solutions. N means number of events.

REGION	AREA OF COVERAGE	February - November 1972			January 1973 - March 1975		
		50%	90%	N	50%	90%	N
1	Aleutians-Alaska	135	330	157	110	220	461
2	Western North America	185	310	39	130	260	129
3	Central America	430	830	61	200	590	146
4	Mid-Atlantic Ridge	360	790	31	150	420	143
5	Mediterranean-Middle East	220	650	120	300	610	389
6	Iran-Western Russia	150	580	76	170	710	182
7	Central Asia	105	270	120	120	300	349
8	Southern-Eastern Asia	130	340	42	150	290	205
9	Ryukuo-Philippines	195	610	166	200	540	424
10	Japan-Kamchatka	95	260	255	100	230	1062
11	New Guinea-Hebrides	380	1330	87	210	840	263
12	Fiji-Kermadec	310	910	183	230	640	508
13	South America	390	680	33	210	495	112
14	Distance Range 30°-90°	145	490	1191	130	310	3775
15	Distance Range 110°-180°	320	1020	409	220	670	1195

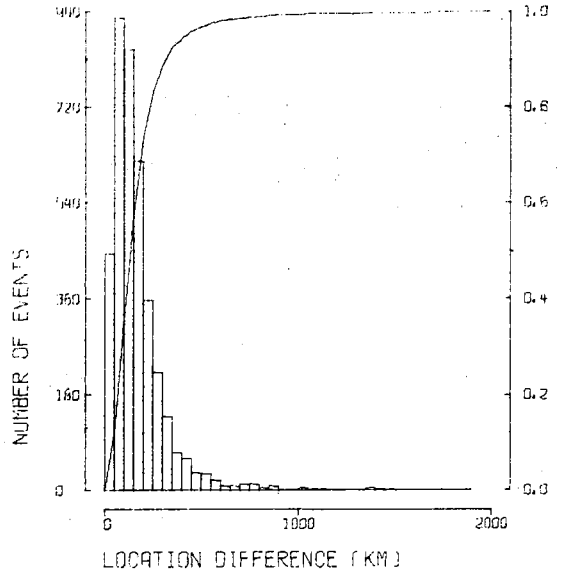

Fig. VII.5.1 Cumulative and incremental distribution of epicenter location difference between USGS and NORSAR for region 14 (distance 30-90 degrees from NORSAR) for January 1973 until March 1975.

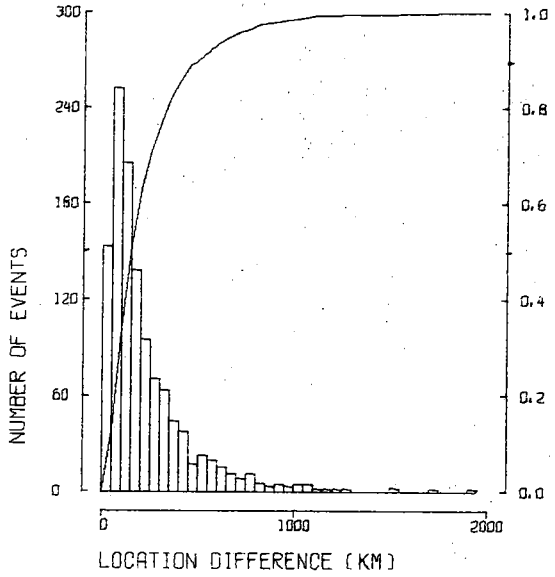

Fig. VII.5.2 Same as VII.5.1 for the time period February to November 1972 (from Bungum and Husebye, 1974).

VII.6 Event Detectability of Seismograph Stations in Fennoscandia

Based on six years of ISC data (1964-69) the operational event detection capabilities have been analyzed for those stations in Fennoscandia that reported regularly to the ISC during this time period (Pirhonen et al, 1976). It has been demonstrated that the incremental P-wave detection probability of a station as a function of ISC m_b can be very accurately modelled by a cumulative Gaussian distribution function. This has been found to hold true when analyzing large as well as small regions. By maximum likelihood estimation based on the Gaussian model (Ringdal, 1975) we have established that operational detection thresholds, both at the 50 and 90 per cent levels, exhibit large variations between individual Nordic stations. For the entire teleseismic region, the 50 per cent thresholds range from m_b=4.5 to 5.5; the best stations being located in Finland. This is consistent with the expected increase in seismic noise level with decreasing distance from the North Atlantic Ocean. Fig. VII.6.1 shows the 50 per cent thresholds of all stations in the teleseismic range, while Fig. VII.6.2 shows the estimated detection curves.

Studies of the noise power spectra of four Fennoscandian stations over a one-year period show as a common feature a very sharp fall-off with increasing frequency in the band of interest for P-wave detection. From 1 to 2 Hz the decrease in average noise power is 15-20 dB, while the standard deviation at each frequency in this band is much lower, typically 4-6 dB.

An attempt to predict relative detectability thresholds based on noise level and station magnitude corrections was only partly successful. The results were generally consistent with previous estimates, but with occasional deviations of several tenths of an m_b unit. The simple method of estimating

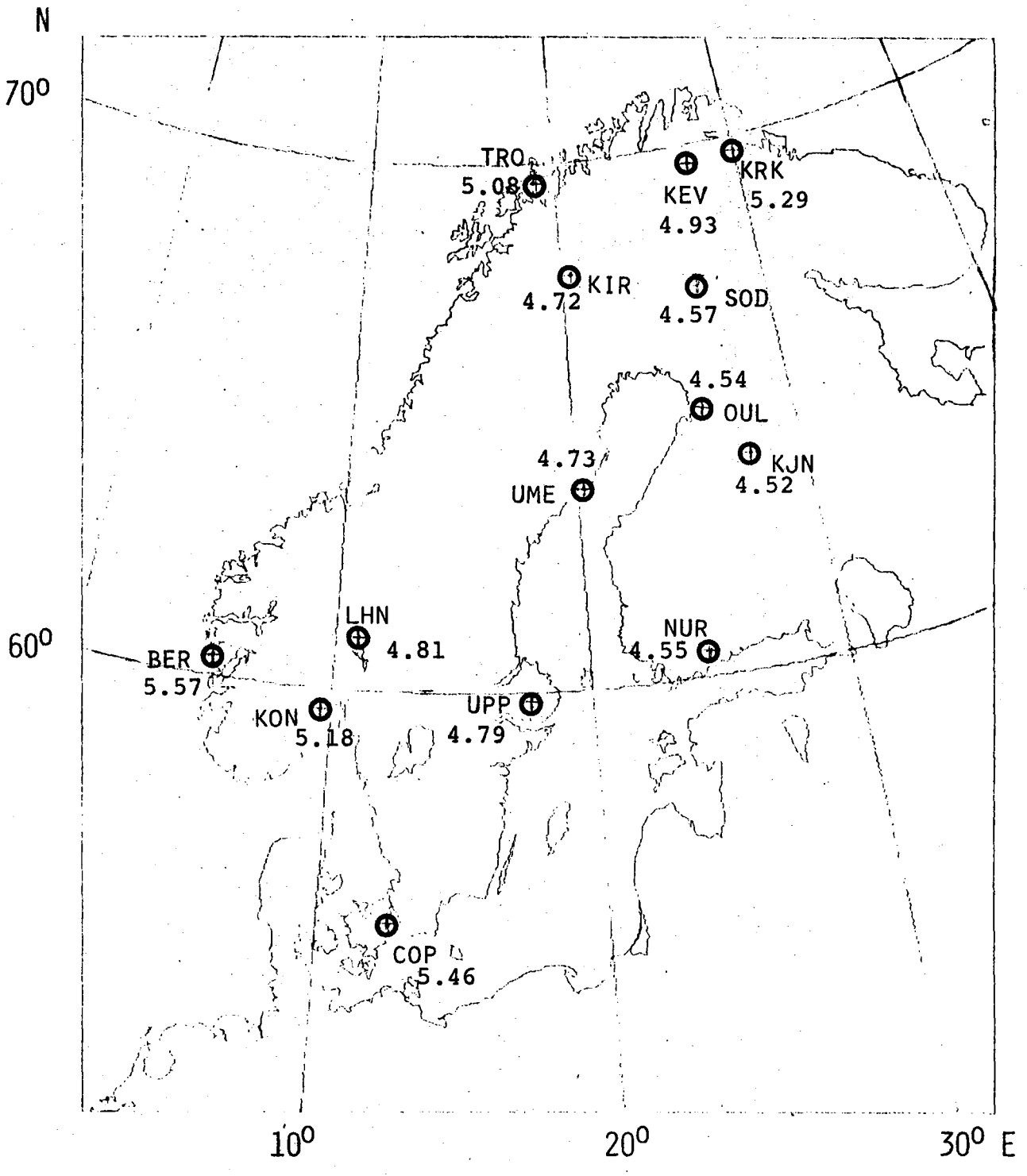

Fig.VII.6.1 Seismograph stations in Fennoscandia used in this study and their estimated 50 per cent operational detection thresholds in the teleseismic range.

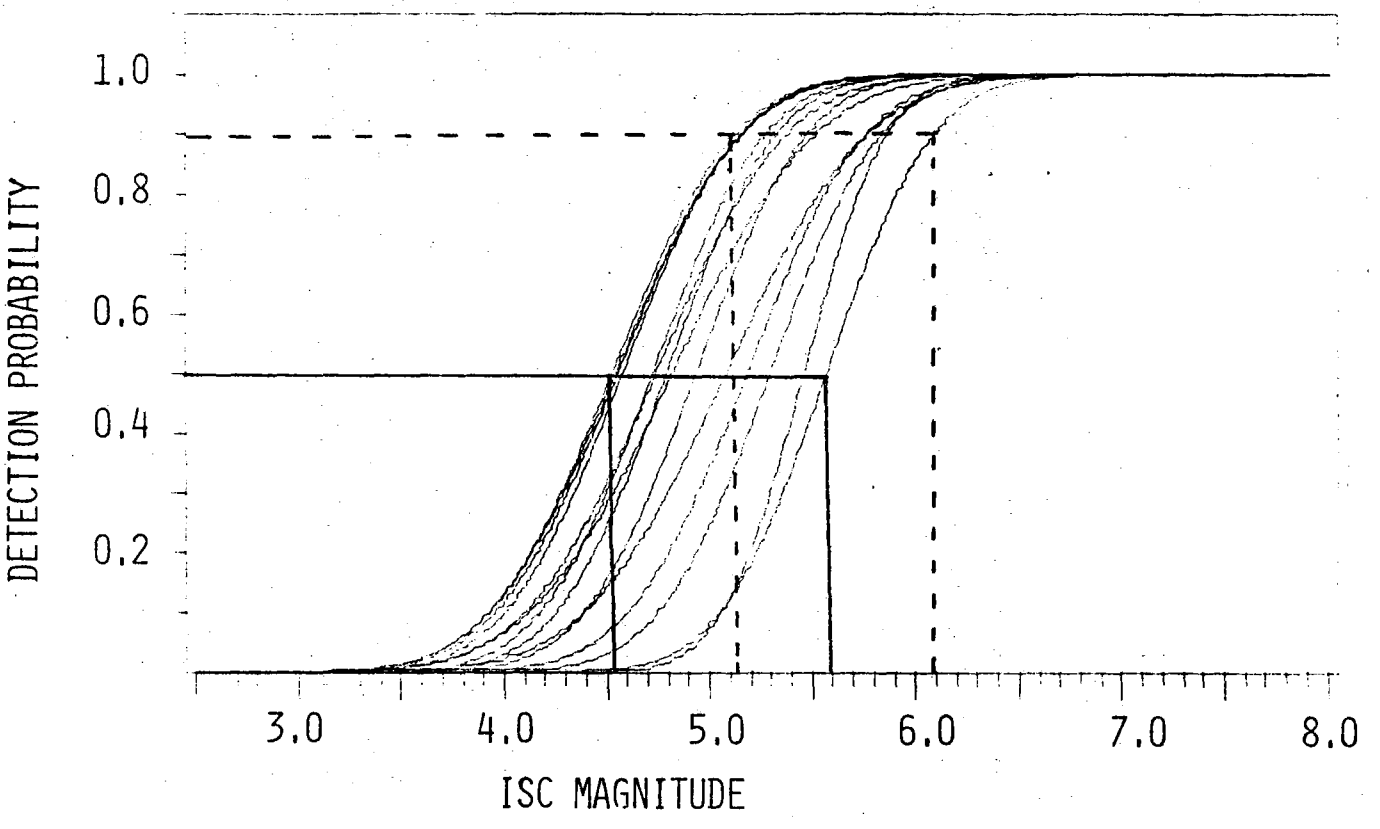

Fig. VII.6.2 Maximum likelihood detectability curves of all stations in the teleseismic range (30-90 degrees from Umeå).

station detecting capability by counting the number of reported events was found to give a good first order estimate of relative 50 per cent thresholds between stations.

For each station, there are significant regional variations in detection thresholds that cannot be attributed to differences in epicentral distances. Of particular interest is the observation that the 50 per cent threshold on the average is 0.4 m_b units higher for Western North America than for the Japan-Kuriles-Kamchatka arc, although the epicentral distances are similar for these two regions. This points to a considerably stronger attenuation of high frequencies in the mantle for the paths corresponding to the former region.

An indirect argument was used to compare the performance of the Fennoscandian stations to the average ISC station for one selected region (Japan-Kuriles-Kamchatka). It appears that the Fennoscandian stations are generally better than average for this region, with a mean improvement in 50 per cent thresholds of about 0.4 m_b units. A more complete evaluation of the relative standings of individual stations in the world-wide network would require a much more extensive study, but could possibly be obtained using the general techniques described previously in this paper.

S. Pirhonen (Helsinki)
F. Ringdal
K.A. Berteussen

REFERENCES

Pirhonen, S., F. Ringdal and K.A. Berteussen (1976): Event detectability of seismograph stations in Fennoscandia, in preparation.

Ringdal, F. (1975): On the estimation of seismic detection thresholds, Bull. Seism. Soc. Am., 65, (in press).

VII.7 On the M_s-m_b Relationship of Earthquakes

The purpose of this study is to estimate the M_s-m_b relationship using data from VLPE, ALPA, NORSAR and PDE, and assess the impact of network magnitude bias effects (Ringdal, 1976) on the results. We assume that there exists a linear functional relationship between M_s and m_b of shallow earthquakes of the form

$$M_s = \alpha \cdot m_b + \beta + \varepsilon \qquad (1)$$

where α and β are unknown coefficients and ε is a random variable that is normally distributed with zero mean and an unknown variance. Generally, the formula (1) can only be used as an approximation over limited magnitude ranges; for example, Gutenberg and Richter (1956) estimate α=1.6 using only very large events, while Evernden (1975) finds a value of α=1.0 below magnitude m_b=5.0 down to at least m_b=3.0.

This study is restricted to the magnitude range of most interest for current seismic discrimination studies, i.e., approximately m_b=4.0 to 6.0. The data base consists of 52 randomly selected shallow Eurasian earthquakes (Turnbull et al, 1975). Magnitudes of these events have been available from PDE and NORSAR (m_b), and from VLPE, ALPA and NORSAR (M_s). In addition, we used the maximum-likelihood technique of Ringdal (1976) to modify the PDE m_b estimates; we denote these modified estimates by PDE(m-l) m_b values. The assumptions required to obtain the PDE(m-l) estimates are described in detail by Turnbull et al (1975).

In order to examine the variations of the M_s-m_b slope as a function of estimation techniques of M_s and m_b, a total of nine cases were run based on the given event population. In each case, the M_s values estimated by either VLPE (averaging), ALPA or NORSAR were combined with the m_b values

of NORSAR, PDE and PDE(m-l). One case is shown in Fig. VII.7.1, while complete results are summarized in Table VII.7.1. The following points are noteworthy:

1. Four of the runs produce a virtually identical slope ($\alpha \approx 1.37$). These are precisely those four runs that combine "consistent" M_s and m_b values, i.e., values free of network bias effects. (NORSAR or ALPA M_s versus NORSAR or PDE(m-l) m_b).
2. A consistently high value of the slope (1.66 or 1.64) is found when PDE m_b is plotted against a consistent M_s.
3. A consistently low value of α (1.23 or 1.24) results when VLPE M_s is plotted against a consistent m_b.
4. When PDE m_b is plotted against VLPE M_s, α is again high, showing that the network bias effects in PDE magnitudes dominate those of VLPE.

Hence, the behavior of the computed slope agrees well with what could be expected from network bias considerations (network magnitude are expected to produce a bias that is largest for small events). It appears that the most accurate linear functional relationship between M_s and m_b for the given data set (ranging in m_b values from about 4.0 to 6.0) has a slope of approximately 1.4.

Considering more closely the four cases of consistent estimates, it is interesting to note that the value of the orthogonal standard deviation σ is lower when using PDE(m-l) m_b versus either ALPA or NORSAR M_s compared to when NORSAR m_b is used ($\sigma \approx 0.26$ vs $\sigma \approx 0.31$). It would be interesting to compare PDE(m-l) m_b to the VLPE-ALPA-NORSAR combined network with the network bias reduced by maximum likelihood processing; however, we have not been able to do this, mostly because of the lack of reliable VLPE data for some stations.

F. Ringdal

L.S. Turnbull (Texas Instruments, USA)

REFERENCES

Evernden, J.F. (1975): Further studies on seismic discrimination, Bull. Seism. Soc. Am., 65, 359-391.

Gutenberg, B., and C.F. Richter (1956): Magnitude and energy of earthquakes, Ann. di Geofis., 9, 1-15.

Ringdal, F. (1976): Maximum-likelihood estimation of seismic magnitude, Bull. Seism. Soc. Am. (in press).

Turnbull, L.S., D. Sun, J. Battis and F. Ringdal (1975): Near and far field studies, Semiannual Report 5B, Texas Instruments Incorporated, Dallas, Texas.

Table VII.7.1

Estimated relationship M_s-m_b for various combinations of M_s and m_b measurement procedures.

m_b	M_s	No. of Points* NP	Slope α	Intercept β	σ Orthogonal
PDE	VLPE	52	1.54	-3.58	0.238
	ALPA	41	1.66	-4.33	0.253
	NORSAR	35	1.64	-3.95	0.276
PDE Maximum Likelihood	VLPE	52	1.23	-1.73	0.262
	ALPA	41	1.37	-2.57	0.257
	NORSAR	35	1.37	-2.25	0.259
NORSAR	VLPE	52	1.24	-1.67	0.309
	ALPA	41	1.37	-2.48	0.321
	NORSAR	35	1.39	-2.14	0.305

* The missing data points (NP<52) are due to lack of available data for NORSAR or ALPA M_s for some events, and not due to nondetection at these stations.

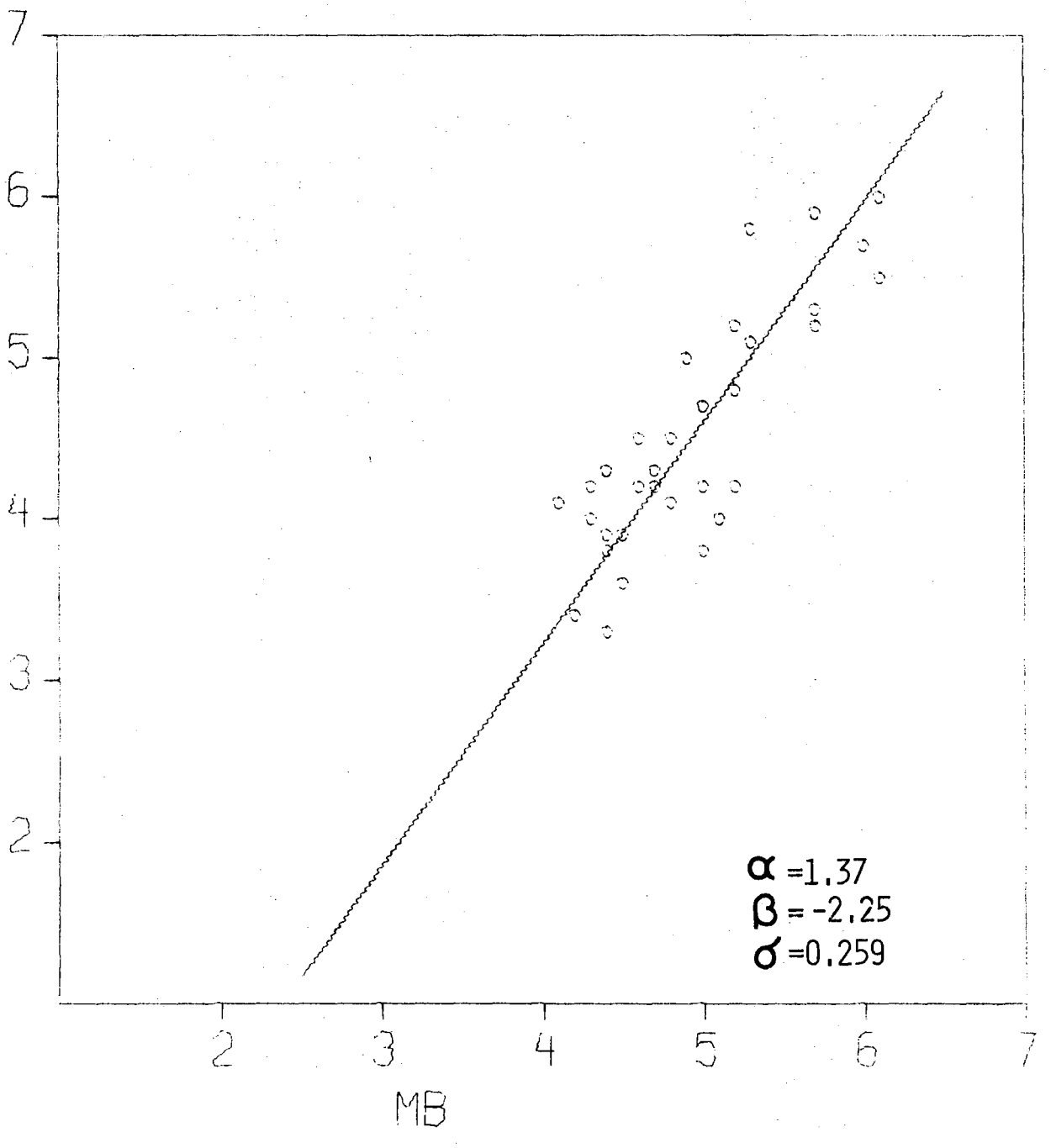

Fig. VII.7.1 PDE m_b modified by maximum likelihood processing plotted against NORSAR M_s.

VII.8 An Improved Discriminant using Spectral Estimates for Surface Waves

In Bungum and Tjøstheim (1976) an improvement of the m_b:M_s discriminant was obtained by combining the m_b:M_s data with some parameters resulting from modelling the short period data, noise as well as main signal and coda, as 3rd order autoregressive time series. The new two-dimensional Z1:Z2 discriminant was defined as

$$\begin{aligned} Z1 &= m_b - 0.4\ \hat{a}_1(S) \\ Z2 &= M_s + 0.4\ (\hat{a}_1(C) - \hat{a}_1(N)) \end{aligned} \qquad (1)$$

where $\hat{a}_1(S)$ is the first order autoregressive coefficient from the main signal and C and N denote coda and preceding noise respectively.

We have now investigated the effect of replacing the surface wave magnitude M_s by a long period power spectrum estimate. More precisely, we adopted $\hat{P}_{20}$, the value of the estimated spectral density (using maximum entropy spectral estimation over suitable group velocity windows) at a period of 20 sec as an estimate of the incoming energy. Using correction formulae for ordinary M_s measurements, we constructed the distance corrected energy estimates

$$E_{20} = \tfrac{1}{2} \log_{10}(\hat{P}_{20}/\pi^2) + 1.66 \log_{10}(\Delta)$$

for distances Δ larger than 25° and

$$E_{20} = \tfrac{1}{2} \log_{10}(\hat{P}_{20}/\pi^2) + \log_{10}(\Delta) + 0.92$$

for distances Δ less than 25°. These quantities were computed for a Eurasian data set consisting of 43 earthquakes and 46 explosions. This data set is identical to the main data set

of Bungum and Tjøstheim (1976) with the exception of two earthquakes for which no digital long period data could be found. The parameters $\hat{P}_{20}$ and E_{20} were computed not only for Rayleigh (RV) vertical component waves but also for Rayleigh (RH) radial component waves and Love (L) transverse component waves. Furthermore, a number of different group velocity data windows were used. The information of interest for discrimination purposes is summarized in Table VII.8.1, where mean values have been computed for three of the windows studied. On the basis of the information in this table we constructed the quantities

$$Y2 = E_{20}^{(1)}(\text{Love}) + (E_{20}^{(2)}(\text{Love}) - E_{20}^{(3)}(\text{Love})) \qquad (1)$$

where the superscripts refer to the windows used. Replacing M_s with Y2 we arrive at the X1:X2 discriminant given as

$$\begin{aligned} X1 &= m_b - 0.4\ \hat{a}_1(S) \\ X2 &= Y2 + 0.4(\hat{a}_1(C) - \hat{a}_1(N)) \end{aligned} \qquad (2)$$

Our results indicate that the discriminant (2) works significantly better than the discriminant in Bungum and Tjøstheim (1976). In Figs. VII.8.1 and VII.8.2 the discriminant (2) is compared with the m_b:M_s discriminant. The m_b:M_s diagram has two explosions within the earthquake population and the separation between earthquakes and explosions is not particularly good. In the X1:X2 diagram these two events are now moved well into the explosion population and the separation between the two populations is substantially improved.

Dag Tjøstheim
Eystein Husebye

REFERENCES

Bungum, H., and D. Tjøstheim (1976): Discrimination between Eurasian earthquakes and underground explosions using the m_b:M_s method and short period autoregressive parameters, Geophy. J.R. Astr. Soc., in press.

Table VII.8.1

The mean values of the energy estimates E_{20} and of surface wave magnitude M_s as obtained by averaging over the 46 explosions and 43 earthquakes respectively.

	1	2	3
Group Velocity Windows (km/s)	8.0-2.2	3.3-2.7	4.2-3.4
$\overline{E_{20}}$ Rayleigh vertical, explosions	3.88	3.89	3.61
$\overline{E_{20}}$ Rayleigh vertical, earthquakes	4.48	4.56	4.05
$\overline{E_{20}}$ Rayleigh horizontal, explosions	3.85	3.81	3.54
$\overline{E_{20}}$ Rayleigh horizontal, earthquakes	4.40	4.47	3.99
Group velocity windows (km/s)	8.0-2.2	3.7-3.1	4.6-3.8
$\overline{E_{20}}$ Love, explosions	3.77	3.76	3.51
$\overline{E_{20}}$ Love, earthquakes	4.55	4.69	4.00
$\overline{M_s}$, explosions		3.72	
$\overline{M_s}$, earthquakes		4.39	

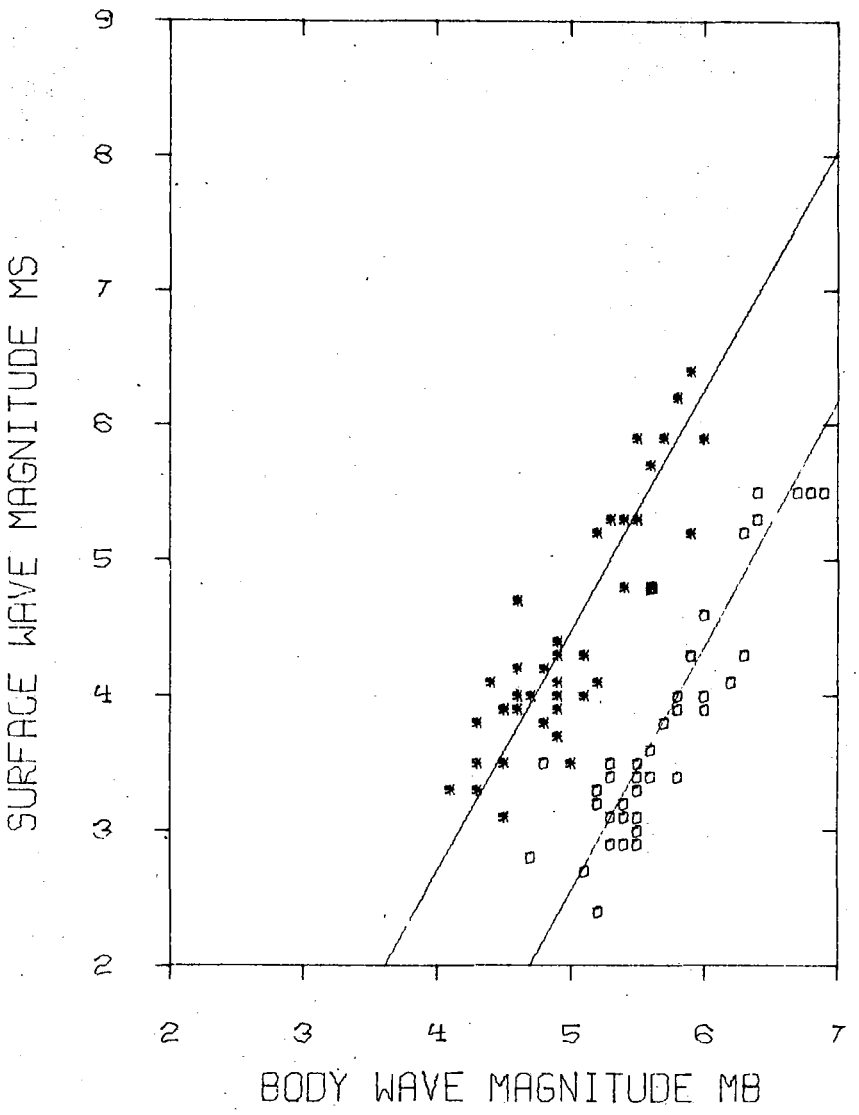

Fig. VII.8.1 m_b:M_s diagram for the 46 explosions and 43 earthquakes. PDE m_b and NORSAR M_s values (rounded to the first decimal) have been used. The regression lines have been fitted using the same maximum likelihood procedure as in Bungum and Tjøstheim (1976).

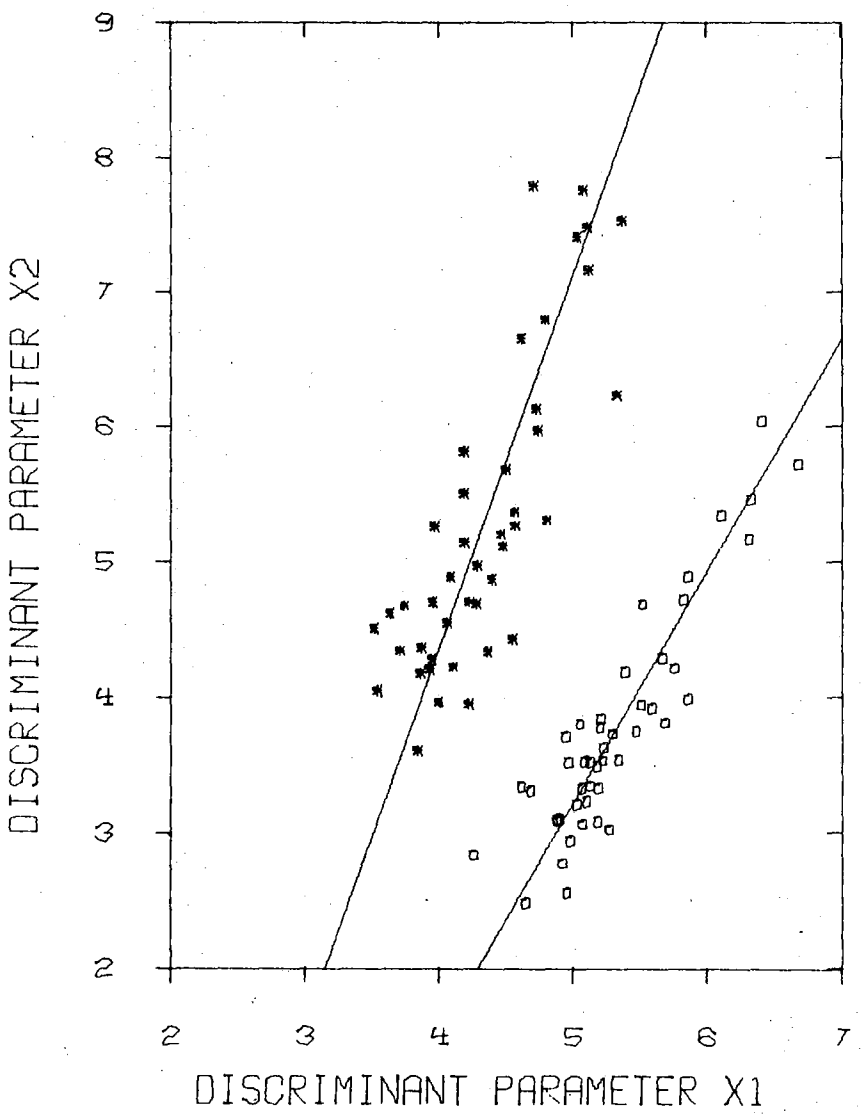

Fig. VII.8.2 X_1:X_2 diagram for the 46 explosions and 43 earthquakes.

VII.9 The Seismicity of Fennoscandia

A critical parameter in seismicity studies is the space-time relationship between the largest occurring earthquakes within the region under investigation. An interesting feature here is that most of the largest shocks ($M \geq 6$) are restricted to the period 1863-1913, while 3 other strong earthquakes took place between 1819 and 1836. There is no indication of spatial migration in the distribution of the largest earthquakes and neither do we find any clear regularity in occurrence of large events in specific areas. In other words, the very largest earthquakes observed seem to be isolated phenomena. This points towards exceptionally long recurrence intervals, i.e., a large time lag between two large events occurring within a tectonically uniform area. As it is considered unlikely that any major earthquake occurring after 1600 are left unreported, the recurrence interval is probably larger than 350 years for earthquakes with magnitude M larger than 6.

The seismicity pattern of Fennoscandia is somewhat diffuse, which is normal for intraplate earthquake occurrence (Sbar and Sykes, 1973). We found it convenient to subdivide the Fennoscandian earthquakes in 3 primary zones: namely, the western Norway zone, the Telemark-Vänern zone and the Bothnian zone; plus a weaker one called the Lappland zone (Fig. VII.8.1).

The western Norway seismicity belt is in northern Norway confined to the coastal area while the epicenters become more dispersed south of 64°N. The west coast area of Norway is relatively prominent seismically and also geophysically (Husebye et al, 1975). A characteristic feature here is that this zone is within the Caledonides and its strike direction is parallel to the folding axis; this can be taken as evidence for the importance of remnant or locked-in stresses from the above mountain folding period. Another feature is that the epicenters are mainly confined to the coastal areas where the relief is very pronounced, which in turn may indicate additional loading stresses and/or zones of weakness.

The Telemark-Vänern seismicity zone which represents a geographical envelope of earthquake epicenters in this area is typified by graben structures and the most prominent one is the Oslo Graben. A slight clustering of epicenters can be found around the mentioned graben structures, pointing towards a causal connection between these structures and earthquake occurrence, possibly through release of locked-in stresses. An alternative explanation is, however, that the orientation of the Telemark-Vänern belt is in fact tectonically significant.

The Bothnian seismicity belt, parallel to the Caledonian folding axis, goes from Lake Vättern to the northern end of the Gulf of Bothnia. The latter area has the most pronounced earthquake activity, and there may be a correlation between the relatively strong glacial uplift and the earthquake occurrence in this particular area (Båth, 1953). ALso, this zone is characterized by faulting.

The Lappland seismicity zone is only weakly defined by the data available to us, but a series of earthquakes in 1973/74 was entirely within this zone. As this area always has been thinly settled, the macroseismic information available would necessarily be scarce.

The above seismic zones account for most of the seismic activity in Fennoscandia during the last five hundred years. The seismic activity is typical for intraplate earthquake occurrence, by neither exhibiting a too clear spatial zoning nor an obvious correlation with geological and geophysical information pertinent to the area. The likely reason for this is that Fennoscandia has been through several tectonic cycles, which in turn is reflected in the present complex stress distribution. Consequently, an improved understanding of the on-going seismic activity here and at the same time a better assessment of dominant stress sources requires more in-situ stress measurements. Equally important would be focal mechanism solutions for earthquakes occurring within Fennoscandia.

E.S. Husebye
H. Bungum

REFERENCES

Bungum, H., and E.S. Husebye (1976): The seismicity of Fennoscandia, submitted for publication.

Båth, M. (1953): Seimsicity of Fennoscandia and related problems, Gerlands Beitr. Geophysik, 63, 173-208.

Husebye, E.S., H. Gjøystdal and H. Bungum (in press): Earthquake activity in Fennoscandia between 1497 and 1973 and intraplate tectonics, submitted for publication.

Husebye, E.S., H. Gjøystdal, H. Bungum and O. Eldholm (1975): The seismicity of the Norwegian and Greenland Sea and adjacent continental shelf areas, Tectonophysics, 26, 55-70.

Sbar, M.L., and L.R. Sykes (1973): Contemporary compressive stress and seismicity in eastern North America: an example of intra-plate tectonics, Bull. Geol. Soc. Am., 84, 1861-1882.

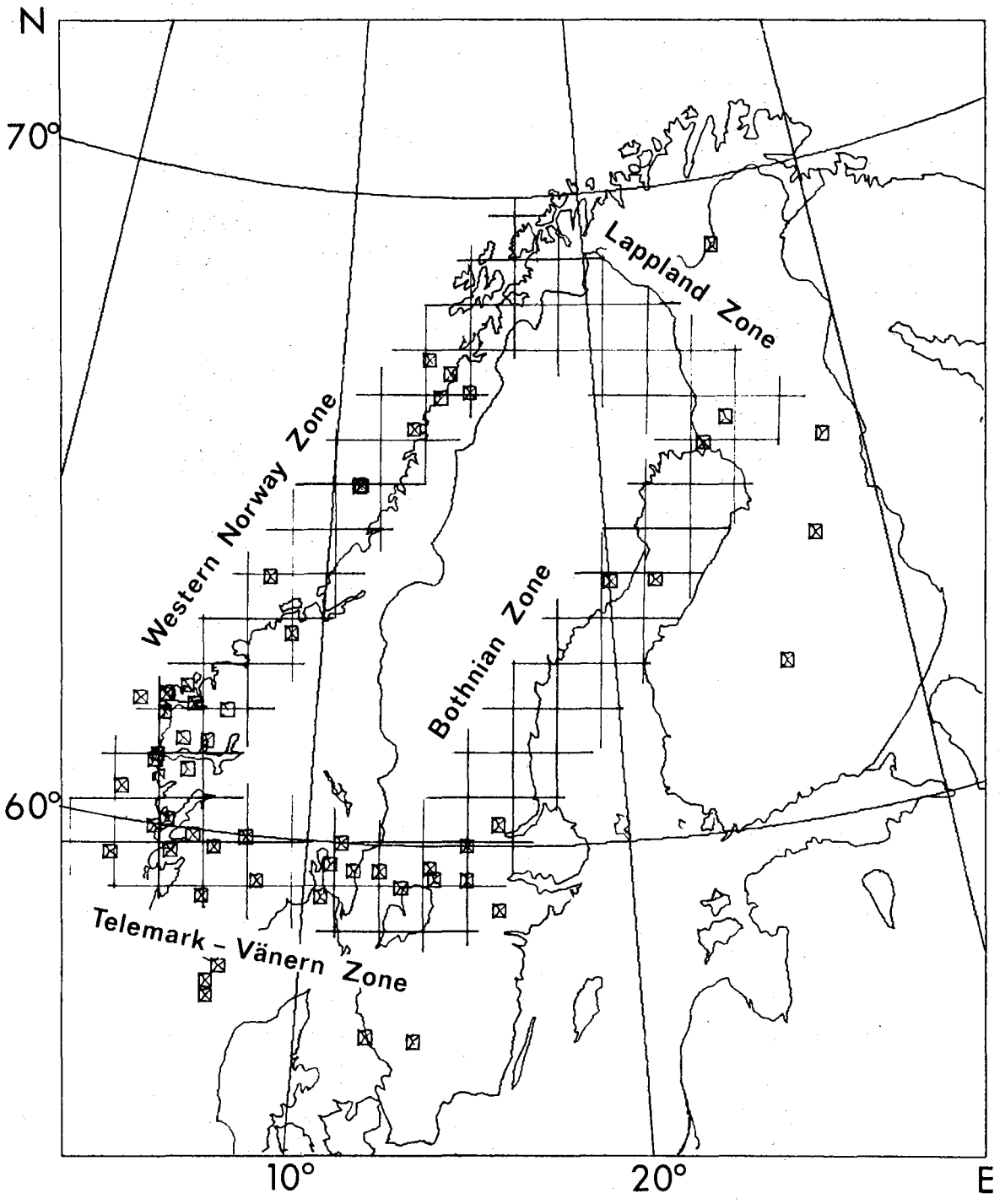

Fig. VII.9.1 Fennoscandian earthquakes for the time period 1497-1973 and with a magnitude M greater than 4.5. An outline is also given of the 4 seismicity zones defined in this paper. Note that the definition of the zones is based on much more seismicity data than is actually displayed in this figure.

VII.10 Precise Monitoring of Seismic Velocities

The physical setup for this experiment was explained in the previous report in this series (NORSAR Scientific Report No. 5-74/75). It involves a power station as a source vibrating at frequencies around 2.778 Hz, 5 seismometers (Ch 1-4 and 6 at subarray 14C), at distances from 4.7 to 13.7 km from the source, and a 6th data channel (Ch 5) where the network power of 50 Hz is input after being divided 18 times down to 2.78 Hz and properly reduced in voltage (to $\pm$4.6 V).

An extensive analysis has now been completed involving about 120 hours (5 days) of data. We have Fourier-analyzed altogether 425 blocks each of 10 000 samples of 10 Hz data (16 2/3 minutes per block), giving a frequency resolution of 0.001 Hz. For each block, the reference channel (Ch. 5) was first analyzed so as to find out what frequencies to analyze, which is important because the network power frequency actually fluctuates as much as $\pm$0.3% around the nominal frequency, with a correlation time of sometimes only a few seconds. This corresponds to frequencies in the range 2.771 to 2.785 Hz, where our resolution gave 15 independent estimates. For each block, we then analyzed any frequency in that range at which the reference channel had stayed for at least 7% of the time, usually giving between 3 and 6 frequencies. Having established the frequencies to analyze in this way, the initial analysis involved estimating the Fourier transform for each of the 5 seismic data channels for each of the selected frequencies. These basic Fourier Transform results were then stacked on a digital tape, ready for subsequent analysis.

The way to monitor seismic velocities from these data is through the analysis of spectral phase differences. We will here only discuss 3 of the many possible combinations, namely, between the source (Ch 5) and Ch 4 (distance 13.7 km), between the source and Ch 1 (distance 4.7 km), and between Ch 1 and Ch 2. The latter two channels are the ones closest to the

source and therefore with the best signal-to-noise ratio, they have also practically the same distance to the source and are consequently essential as a control combination.

The phase estimates in Fig. VII.10.1 are obtained by summing the power spectral estimates over all the analyzed blocks of data, after some reduction. For each of the frequencies in each of the blocks we analyzed the power in the reference channel. It has been found that the quality of the phase estimates is proportional to this power level, and consequently a threshold was determined below which the data was rejected. In this way we improved the quality of the phase estimates by rejecting about 40% of the original data; in Fig. VII.10.1 it is shown that there remains between 1 and 146 blocks for each of the frequencies.

An important by-product of the phase estimates in Fig. VII.10.1 is that they actually give, albeit with considerable uncertainty, an estimate of the group velocity, either between two seismometers or between any seismometer and the source. The slope $d\phi/d\omega$ has been estimated using a weighted least squares estimation procedure, using as weights the number of blocks for each frequency (since that number is directly proportional to the stability). Once the slope is estimated, the group velocity is simply the distance divided by the slope. The group velocity results are not really as consistent as could be the impression from Fig. VII.10.1 ($v = 3.9 \pm 0.6$ and 3.8 ± 0.4 km/s); for the combinations of channels with acceptable signal-to-noise ratios the estimates actually vary between 3.0 and 5.0 km/s. However, using the group velocities arrived at in this way, and assuming the same values for the phase velocities, it is possible to estimate the total travel time and thereby the relative size of observed phase differences. It is found in this way that a precision of $\pm 10^{-3}$ for combination 1-5 corresponds to $\pm 1.2^{\circ}$, and for 4-5 the value is $\pm 3.6^{\circ}$, corresponding to the error bars in Fig. VII.10.1.

An obvious way to further improve the stability of the phase estimates is to use, instead of the values for individual frequencies, the intercept of the regression line with the center frequency. (The error bar in Fig. VII.10.1 has been placed around that value.) That is the technique used in Fig VII.10.2, where each phase estimate is the average over 200 minutes of data. On the average, there are around 30 individual spectral estimates (12 blocks and 2.5 frequencies per block) behind each data point in Fig. VII.10.2. The figure shows that there is no significant time variation in the data, and the standard deviation for combinations 1-5 and 4-5 are 1.5^{o} and 4.0^{o}, respectively, which is quite close to the values given above for a precision of 10^{-3}. The fact that we get the same precision for the two combinations means that the loss in signal-to-noise ratio for the greatest distance is compensated by the increased distance (by a factor of 3). Assuming now that a precision of 10^{-3} is obtained for each of the points in Fig. VII.10.2, we should by summing all the data, obtain a precision of about $10^{-3}/\sqrt{36} \simeq 2 \cdot 10^{-4}$, which refers to the intercept points in Fig. VII.10.1.

This report is only preliminary, and work continues along the following lines: 1) Predict the possible influence from tidal stress variations (the 5 days analyzed here are selected so as to cover a time period when those variations are supposed to be at a maximum), 2) Further improve (by proper data reduction) and more accurately assess (from spectral variances) the precision of the already acquired data base, 3) As a continuation of the project, consider using higher harmonics of the 2.778 Hz data, which have quite good signal-to-noise ratios, and where the phase differences due to tidal effects should be larger.

H. Bungum
T. Risbo (Copenhagen)
E. Hjortenberg (Copenhagen)

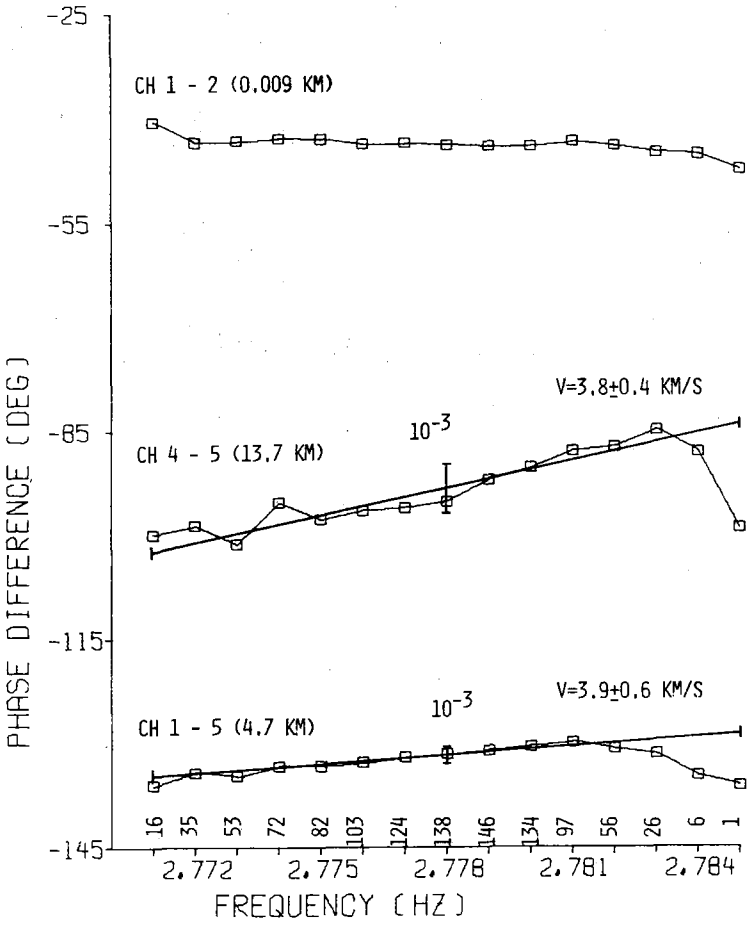

Fig. VII.10.1 Phase difference vs. frequency for three channel combinations, at sub-array 14C. The tilted numbers at the frequency axis are the number of blocks used in each estimate, which have been used as weights in a weighted least squares estimate resulting in the straight lines and the velocities given on the figure. Uncertainty bars of 10^{-3} are also given.

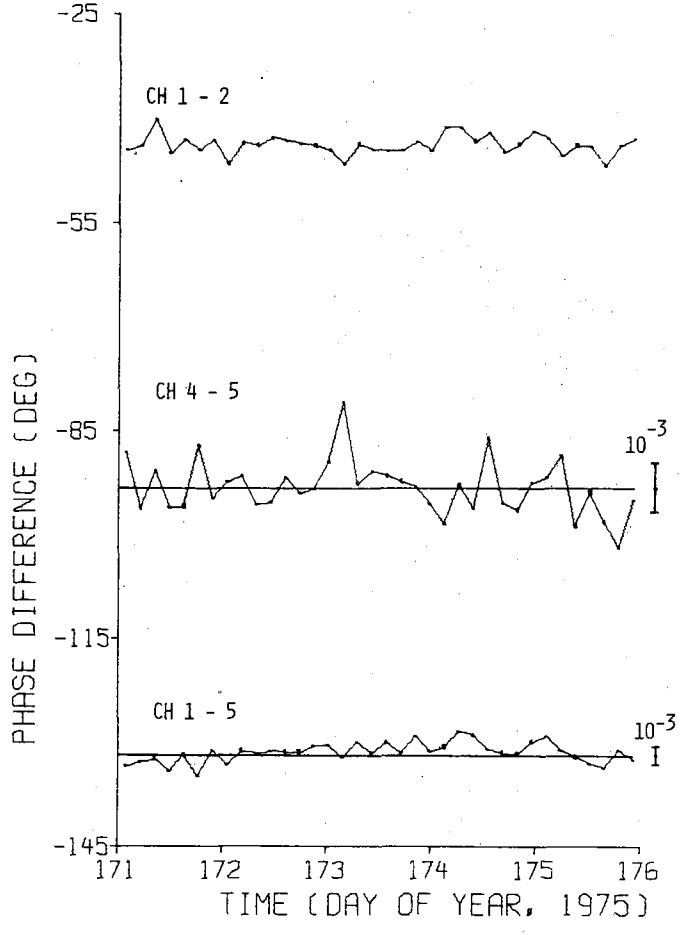

Fig. VII.10 Phase difference vs. time with 36 independent and successive estimates. The channel combinations and the uncertainty bars are the same as in Fig. VII.10.1.